Development and Characterization of Self-Healing Epoxy Systems for Space Applications

Girish Thatte

A thesis

in

The Department

of

Mechanical and Industrial Engineering

Presented in Partial Fulfillment of the Requirements
For the Degree of Master of Applied Science at
Concordia University
Montreal, Quebec, Canada

December 2006

Your file Votre référence
ISBN: 978-0-494-28946-4
Our file Notre référence
ISBN: 978-0-494-28946-4

ABSTRACT

Development and Characterization of Self-Healing Epoxy Systems for Space Applications

Girish Thatte

Composite materials used in space applications are susceptible to damage due to space debris, thermal shock, exposure to UV radiations and atomic oxygen. In space, repair of the damage to space structure is very difficult and in some cases impossible. As such if the micro damage can get healed automatically, it may extend life of space structures.

In the last few years a lot of research has taken place in the field of self-healing of materials. In previous work many different techniques were developed. The majority of these techniques are in their initial stage. The self-healing process can be activated by radiation, addition of chemicals, change in temperature and some without any external assistance. In past work healing efficiency was determined from the critical fracture load of the samples.

This thesis introduces a new monomer for self-healing of materials in space applications. A new approach to determine the healing performance is suggested and different types of environmental conditioning tests were carried out. A finite element model was developed for the calculation of healing efficiency. Finite element results were compared with experimental results.

ACKNOWLEDGEMENTS

The author would like to express his sincere gratitude to his supervisor Dr. Suong V. Hoa and co-supervisor Dr. Philippe G. Merle for their advice, constant guidance and help throughout his graduate studies.

He thanks Dr. Emile Haddad at MPB technologies Inc. for his co-operation and help during this project work.

Investigation of new monomer has been carried out by Yoann Guntzburger. Special thanks to Mr. Yoann Guntzburger for his valuable assistance in this project work.

Also the author extends his thanks to Dr. Ming Xie for his help and co-operation throughout his project.

The author wish to thank Canadian Space Agency (CSA) and MPB Technologies Inc. for financial support and co-operation during this project.

Table of Contents

List of Tables

List of Figures

Nomenclature

$K_{ICvirgin}$	Fracture toughness of the virgin sample
$K_{IChealed}$	Fracture toughness of the healed sample
G	Crack extension force
P	Applied load
a	Crack length,
C	Specimen compliance when the crack length is a
E	Young's modulus
ν	Poisson's ratio
x	Distance along the crack plane measured from the point of loading
h	Specimen height profile
$P_{Cvirgin}$	Critical fracture load of virgin sample
$P_{Chealed}$	Critical fracture load of healed sample
K_{IC}	Fracture toughness
P_c	Critical fracture load
m	Geometric term
β	Geometric term
b	Specimen width
b_n	Crack width
α	Geometric angle

List of abbreviations

5E2N	5-ethylidene-2-norbornene
5V2N	5-vinyl-2-norbornene
MCPD	methylcyclopentadiene dimer
COD	cyclooctadiene
DCPD	dicyclopentadiene
b.p.	boiling point
m.p.	melting point
DSC	Differential Scanning Calorimetry
EMA	Ethylene Maleic Anhydride
M/I ratio	Monomer/Initiator ratio
ROMP	Ring Opening Metathesis Polymerization
rpm	Rotation per minutes
CTE	Coefficient of thermal expansion
Sr. No.	Serial Number
TDCB	Tapered Double Cantilever Beam

Chapter 1

Introduction

1.1 Scope of this work

Composite materials have wide applications due to their favorable properties such as strength and stiffness combined with lightness as compared to metals. They have been used in transportation vehicles, for defense and automobile industry, space exploration and other commercial applications. Figure 1.1 shows the use of carbon fiber reinforced plastics in the construction of the Airbus A380 and Figure1.2 shows uses of composite materials in space applications.

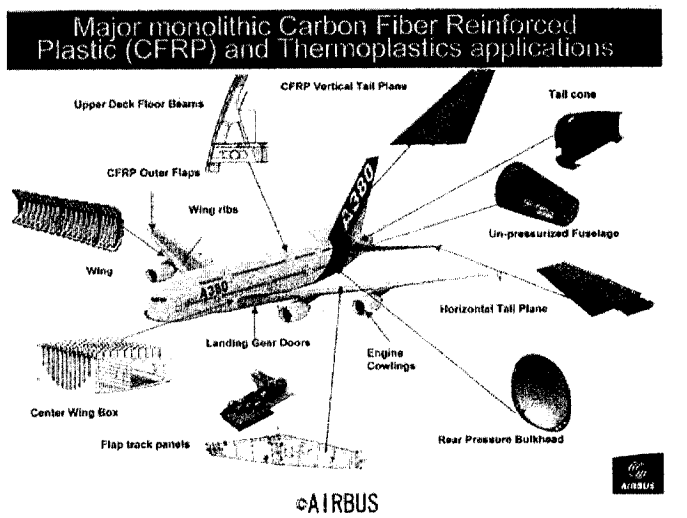

Figure 1.1 Different parts showing the use of carbon reinforced fibers plastics in construction of Airbus 380 [1]

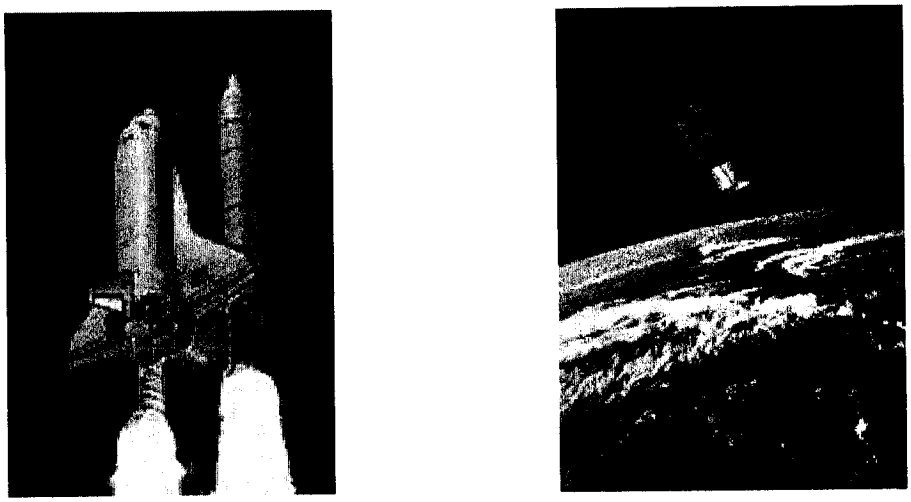

(a) ©NASA (b) ©EADS

Figure 1.2 Application of composite materials in (a) Space shuttle [2], (b) Aeolus Satellite [3]

Figure 1.3 shows different components of satellite such as antenna reflector, bus structures, shielding covers, connecting frames where composite materials are used [4].

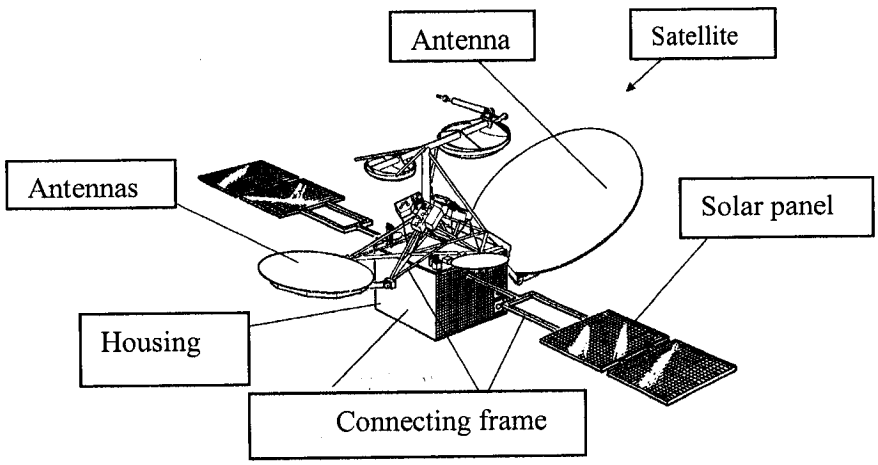

Figure 1.3 Different components of satellite [4]

For spacecraft components such as vehicle nose tip, rocket motor nozzles, electronic packaging propulsion and fuel tank, composite materials are used [5].

Space shuttles and satellites are susceptible to damage due to various reasons, the primary of which is the impact with space debris. In four decades of space activities, there have been some 4000 launches, which have generated a large number of space debris [6]. Out of the 8700 objects larger than 10 cm in Earth orbits only 6 % of that are operational satellites; the remaining being space debris [7]. These space debris and meteoroids can cause severe damage to the spacecrafts. The effect of impact depends on many factors such as the location of the impact, the size, mass, composition and speed of the impacting object as well as impacting angle. Depending upon the severity of all theses factors, the impact effect can be minimal, can degrade the functionality of the spacecraft/satellite component or can compromise their functionality, up to the point where the mission is lost or even worse lives are lost [8].

In addition to this space environment has special parameters such as thermal cycling, high vacuum, atomic oxygen, UV rays etc. Mainly thermal cycling is responsible for matrix expansion and contraction which leads to matrix cracking [9]. Atomic oxygen in upper atmosphere is responsible for the deterioration of spacecraft material and coatings. Plasma and radiation environments are also responsible for the damage to the space shuttle/satellite components [10].

Investigation of damage to the spacecraft/satellite is very difficult at the surface and within the body. This necessitates non destructive testing such as Ultrasonic scanning and X-ray analysis in order to locate and quantify the extent of damage. In space, where inspection and repairing or replacement of a structure is very difficult, expensive and in some cases just impossible, the material which heals itself can become the key technology to repair damages in spacecrafts/satellites.

In the majority of structures a microcrack is the main reason for structural damage. At microcrack, stress concentration occurs and microcrack grows to a macrolevel which ultimately leads to destruction of the structure. As such if there is some technique that can cure microcrack automatically and stop crack propagation to macrolevel, it may avoid further damage to the structure. In this sense self-healing materials have wide scope in the future for space applications.

1.2 Previous state of the art

Although there can be potential benefits of self-healing of materials, only few research teams originated mainly from the US as well as Europe are working on the subject and to the best of our knowledge there is no Canadian team.

Among them, White *et al.* from the University of Illinois at Urbana Champaign (UIUC) have been working on such materials since the mid - 1990s [11]. The group used the concept of biological healing of minor cuts in a skin for the development and investigation of the new material. As shown in Figure 1.4 the group used microcapsules filled with healing material and catalyst for the self-healing of tiny cracks. When damage occurs in a polymer matrix material, a crack propagates through the matrix rupturing microcapsules in a crack path. A ruptured microcapsule releases a healing agent which is drawn in to the crack through capillary action. A healing agent within the crack plane comes into contact with an embedded catalyst and polymerization of healing agent occurs which results in a healed crack [6, 12-16].

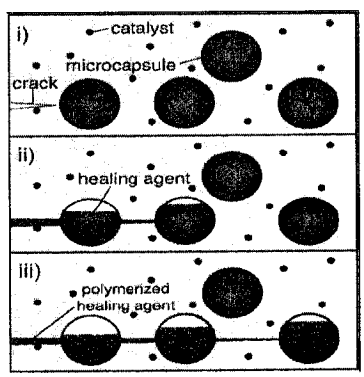

Figure 1.4 Self-healing concept [13]

The healing efficiency was determined considering the critical fracture load of samples. The load vs. displacement graph for neat and self healed sample is shown in Figure 1.5.

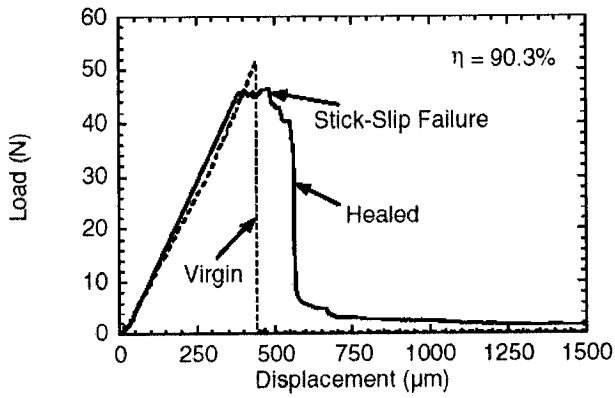

Figure 1.5 Load-displacement graph for virgin and healed sample [15]

Based on the same concept, the group from Bristol University used hollow glass fibers to store functional component for self repair system [9]. A hardener is either microencapsulated or stored in hollow fiber as shown in Figure 1.6.

The group has tried a number of different resin systems and activation methods suitable for space applications. They have selected Cycom 823 epoxy resin system from Cytec Engineered Materials with long shelf life, a viscosity of <250 cP and curing temperature <100 °C for their work [9].

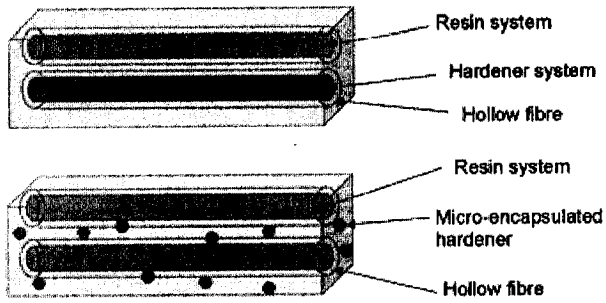

Figure 1.6 Hollow fiber self-healing approach [9]

Fibers were filled with healing agent by vacuum assisted system along with capillary action as shown in Figure 1.7.

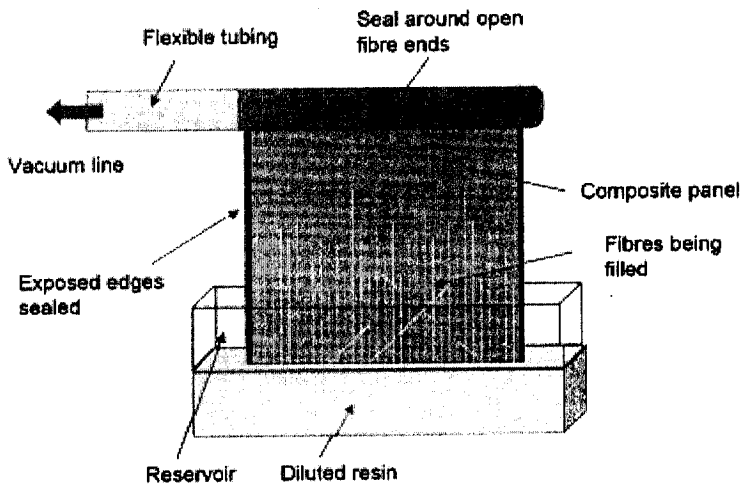

Figure1.7 Schematic diagram of vacuum assisted capillary action fiber filling [17]

Four point bending test was carried out to determine the strength restoration after self repair and the damaged site was observed. UV fluorescent die along with the healing

agent was used for better visualization of fractured site. Figure 1.8 shows bleeding of dye from within the fractured fibers into the damage site.

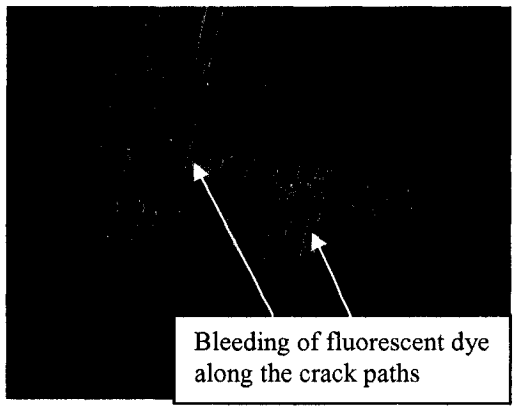

Figure 1.8 Fracture of a hybrid solid/hollow fiber reinforced plastic showing bleeding of UV fluorescent dye along crack paths [18].

A group from Osaka University, Japan [19] used epoxy particles with melting point of 383 - 413 K as a repairing agent. These particles can be melted on the application of heat. The maximum particle diameter was maintained at 50 μm. Glass fibers were used as reinforcement, epoxy resin as a matrix material and epoxy particles as a healing material. On the application of heat the embedded particles in matrix melt and flow to repair the crack (Figure 1.9).

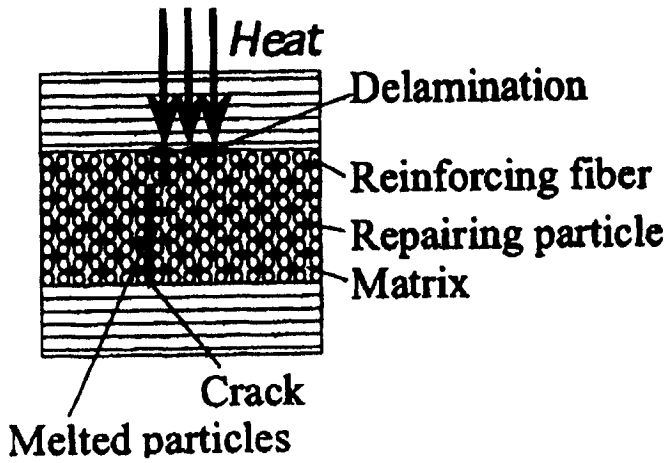

Figure1.9 Repairing particles embedded in to the material as repairing agent [19]

Another contribution of self-healing material originated from Ilhan *et al.* at Princeton University [11]. They have been working on self healing materials which mimic the function of biological healing mechanism just like in plants and animals. Their main area of focus is classical blood clot scenario, using a principle based on electrohydrodynamic (EHD) flow to replicate the same functionality in the synthetic materials. In their test system, a suspension of colloidal particles is enclosed between the walls of a double walled tube. The tube walls are coated with a thin conducting layer followed by an insulating film and are then attached to an electrical power source. The whole assembly acts as an electrode system that can be activated if the insulating film fails. When there is a crack formation in the insulating film, the colloidal particles aggregates (similar to blood coagulation) at the crack site by EHD flow and trigger the first stage of self-healing. The functionality depends upon a continuous electrical field which is analogous to a biological system which relies on a continual sensing mechanism provided by the nerve ending. The test system is shown in Figure 1.10 [11].

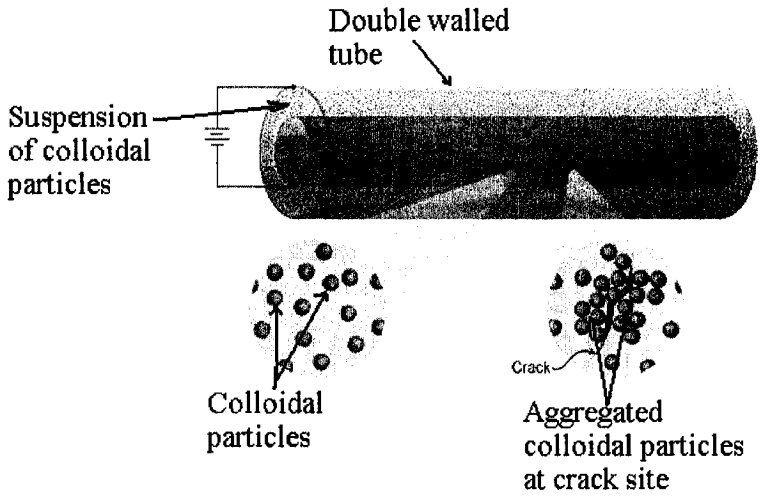

Figure 1.10 Electrohydrodynamic aggregation of colloidal particles [11]

Another approach was developed by Wudl and his team from the University of California Los Angeles. They went back to the basics of polymer chemistry to create an alternative type of self-mending material. The group developed a transparent organic polymeric material which can mend and re-mend. These materials are solid at room temperature and below, possessing mechanical properties similar to that of epoxy resins. When these materials are heated above 120 °C, approximately 30 % of "intermonomer" linkages disconnect and upon cooling it reconnects. This process is repeatable and can be used to restore a damaged part of the polymer multiple number of times [20]. Figure 1.11 shows a healed crack after heating.

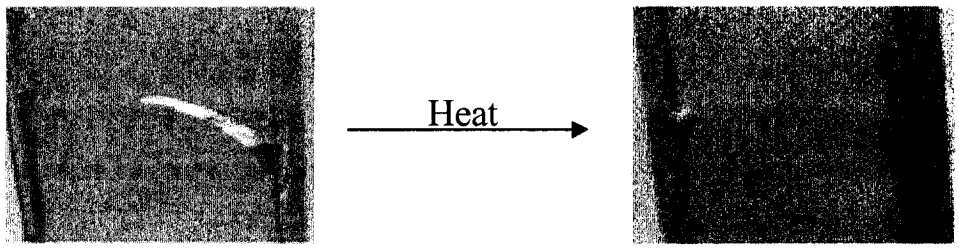

(a) (b)

Figure 1.11 Remendable material showing (a) polymer with shiny crack, (b) crack disappears after thermal healing at 120 °C [21]

Thomas A. P. *et al.* used a polymer with thermo-reversible covalent bond. As shown in Figure 1.12 the braided electromagnetic wires were used for heating purpose within the material. The wires provide channels through which heat is transported to heal cracks within the material. The reinforcing fibers with a negative coefficient of thermal expansion (CTE) were chosen to reinforce the core of the braid or to fill in the weave of the laminate. These fibers provide compression to close the crack faces on the application of heat. Upon heating a cracked polymer matrix having positive CTE will expand as the reinforcing fibers contract putting the matrix into compression and closing the crack faces [22]. In this technique electrical supply or heating arrangement is needed to achieve the healing of crack.

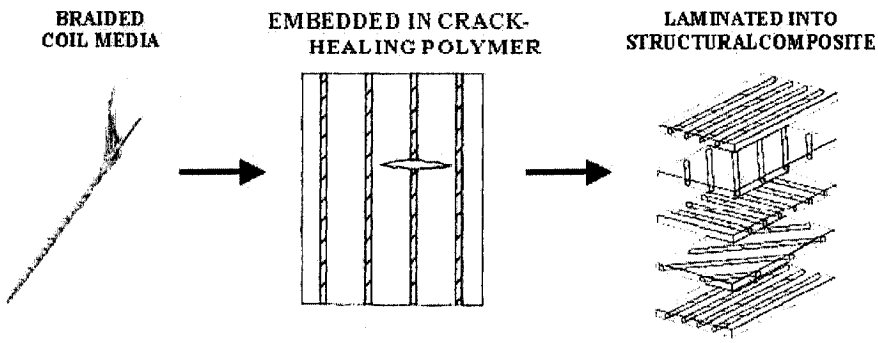

Figure 1.12 Material embedded with the electromagnetic wires for self healing [22].

S. R. White from the University of Illinois Urbana Champaign along with other researchers are doing research on three-dimensional (3D) microvascular networks with pervasive, interconnected channels having diameter less than 300 micrometers. Fluid flow control and mixing are very difficult in microfluidic channels. The group tried to find out a way of fluid mixing at micro level.

The group demonstrated an easy approach for creating fluidic devices based on a 3D microvascular network of cylindrical microchannels. Such channels were directly assembled by robotic deposition of fugitive ink (Figure 1.13) and then patterned to yield vertically oriented, square-spiral mixing towers within the device (Figure 1.14). Owing to their complex architecture, these vertical towers give rise to dramatic improvements in fluid mixing relative to simple straight (1D) and square wave (2D) channels [23].

This technique is in initial stage and was not tried for the self healing purpose.

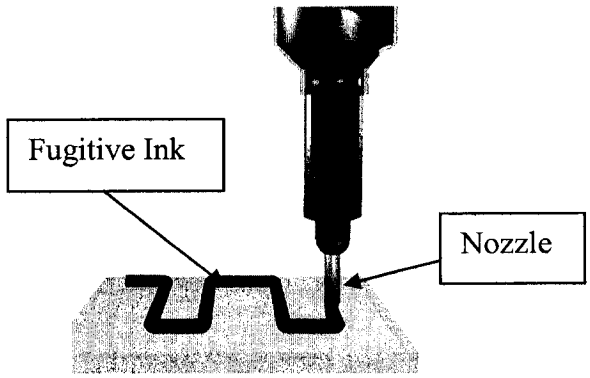

Figure 1.13 Robotic deposition of the fugitive organic ink through a cylindrical nozzle onto a moving *x*–*y* stage [23]

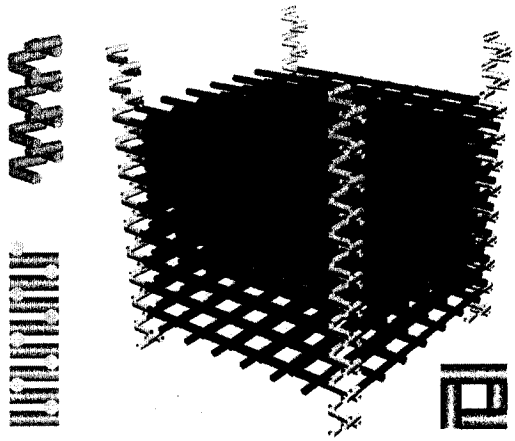

Figure 1.14 Microvascular network [23]

1.3 Limitations of current approaches

Self-healing systems must fulfill some criteria to be successfully used in space application. As discussed in section 1.1, the healing system should be autonomous as external assistance is difficult and in some cases impossible to provide especially in space. Also healing agent should be compatible with space environment with wide liquid temperature range. Based on these criteria the limitations of different self-healing techniques, mentioned in the section 1.2 are discussed here.

The fibers filled with resin and hardener were used by the group from Bristol University for healing purpose. In this technique, the knowledge of exact nature of the damage site within a composite laminate is necessary to incorporate the fibers containing healing agent and hardener. This necessitates some preliminary work to find out damage sites for different orientation of the fibers containing resin and hardener [9].

Ilhan *et al.* from Princeton University [11] have not tested the strength of the tubes after electrohydrodynamic healing process. Though their healing technique is successful they still have to solve another problem as most materials fail because of cracks starting from the outside and working inwards. When healing process starts with this technique, the cracks may have penetrated enough to cause failure to the structure [24].

The remendable materials by Wudl from University of California, containing reversible crosslinked bonds provides a good option as it does not require additional healing material and catalyst [20]. But application of heat is required at damage site to heal the

material. As such this does not justify the term "self-healing" as some external assistance is required to initiate healing process. Similarly, the technique used by the group from Osaka University requires application of heat to the damage site to melt epoxy particles and allow it to flow into damage site to heal the damage.

Use of the microvascular network for self-healing is still in its initial stage. To use this technique for self healing purpose, there are many challenges such as keeping continuous flow of healing material and curing agent in these channels, creation of these channels in complicated shape structure, keeping healing material separate from curing system before damage can occur and the effect of these microchannel networks on the properties of the material are still not resolved.

Among all the techniques discussed in section 1.2, the technique used by the group from University of Illinois at Urbana Champaign was found more effective and autonomous for the healing process; as such this technique was selected for this thesis work. Still the group has not focused on the application of this technique for space application. The DCPD monomer used by the group has the liquid temperature range from 11 to 170 °C. In space where the temperature fluctuation is from -156 to +121 °C, the DCPD monomer may not show the self-healing below the 11 °C. This necessitates the investigation of new monomer. As mentioned previously in section 1.2, the critical fracture load consideration for the determination of healing efficiency may not be proper way as explained in section 4.2. This requires a new method to calculate healing efficiency.

1.4 Objectives

The objective of this thesis is to develop and characterize a self healing epoxy system for space applications.

This includes investigation of new monomer with wide liquid temperature range to replace DCPD. Find new approach to calculate healing efficiency and determine healing efficiency of samples conditioned at different environmental conditions.

Finite element analysis was performed using ANSYS® 10.0 to aid in understanding the efficiency of healing.

Chapter 2

Finding of a new monomer for self-healing composite material

Self-healing technique used by White *et al.* from the University of Illinois at Urbana Champaign is discussed here and its limitations for space applications are described. The possible solution for this problem was found out.

2.1 Current state of the art

As mentioned in section 1.2, White *et al.* from the University of Illinois at Urbana Champaign used microcapsules to store healing agent and catalyst as initiator for polymerization reaction. Figure 2.1 shows schematic diagram of self-healing system containing microcapsules filled with healing agent and catalyst.

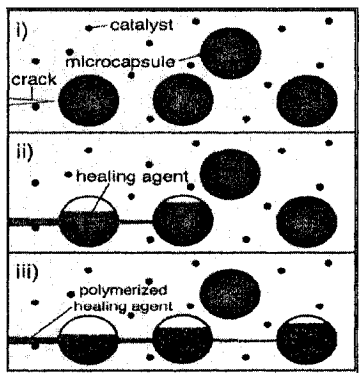

Figure 2.1 Self-healing concept [13]

In the above system Dicyclopentadiene (DCPD) monomer was used as a healing agent and 2.5 % of Grubb's catalyst was used as polymerization reaction initiator. DCPD is in

the encapsulated form and catalyst is in powdered form. DCPD polymerizes through the Ring-Opening Metathesis Polymerization (ROMP). The polymerization reaction between DCPD monomer and Grubbs' catalyst is shown in Figure 2.2.

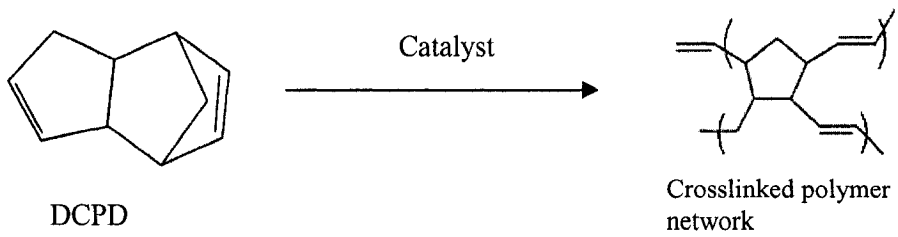

Figure 2.2 Ring Opening Metathesis Polymerization

EPON® 828 epoxy resin and Anacmine® DETA curing agent was used for the sample preparation. For different agitation rates the group found that the diameter of microcapsules varied according to the agitation rate. For their research work, microcapsules with average diameter in the range of 10 - 1000 μm were used for testing purpose by adjusting agitation rate between 200 - 2000 rpm. [25]. Figure 2.3 shows the picture of microcapsules.

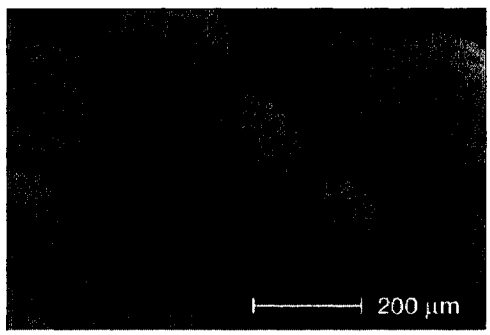

Figure 2.3 Picture of Microcapsules [25]

2.2 Limitations of current material system

DCPD monomer used in the previous technique discussed in section 2.1 was obtained from Acros Organics® (Geel, Belgium) with liquid temperature range of 11 - 170 °C [26].

In this thesis few microencapsulation processes was done with DCPD monomer obtained from Sigma-Aldrich®. The liquid temperature range for this monomer was 33 – 170 °C. As such at room temperature and below DCPD is in solid state. Few microencapsulation tests were carried out and the condition of DCPD monomer inside the microcapsule shell was observed under the microscope. When DCPD microcapsule shell was broken by syringe needle, DCPD monomer in solid state inside the capsule shell was observed as shown in Figure 2.4.

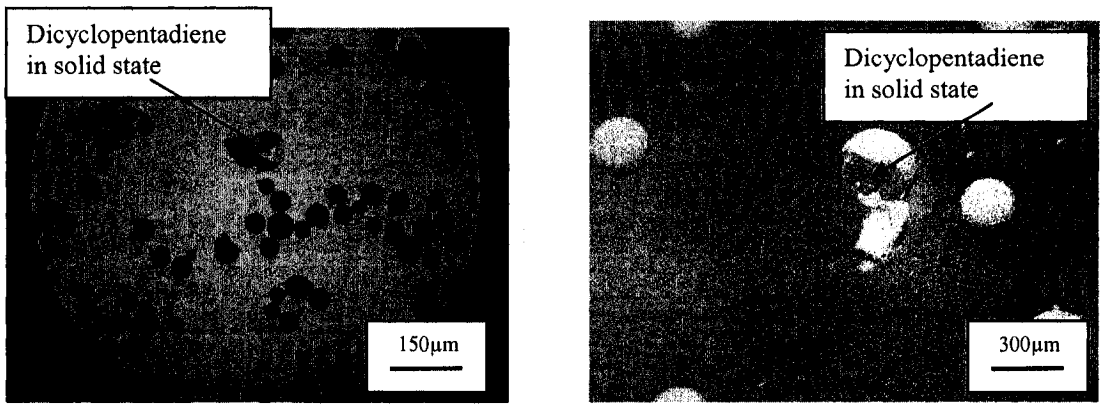

Figure 2.4 DCPD in solid state inside the capsule shell

Due to high melting point of DCPD, below 33 °C it remains unpolymerized in the capsule shell as represented by number '2', leaving the crack unfilled with healing material as shown in Figure 2.5.

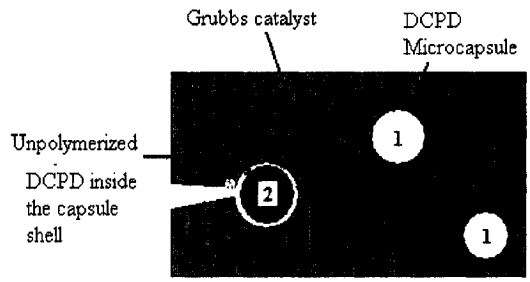

Figure 2.5 Schematic diagram showing unhealed crack

For self-healing of crack, the healing agent must be in liquid state so that it will flow into the crack plane to heal the crack. Figure 2.6 show the healing of crack in which the liquid monomer from the broken microcapsules flowed into the crack plane due to capillary action and polymerized as represented by number '2'.

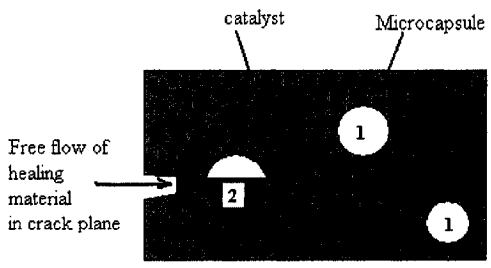

Figure 2.6 Schematic diagram showing healed crack

2.3 Search for a new monomer

As discussed in section 2.2, DCPD monomer is not suitable for the space applications where temperature fluctuation is from -156 °C to +121 °C. This necessitates the investigation of new monomer with a wide liquid temperature range and compatible to space environment.

Besides having free flowing property, the monomer should also fulfill the following requirements, to be used as a healing material for space applications.

- Monomer should have a wide liquid temperature range (covering room temperature)
- The new monomer should be able to undergo a Ring Opening Metathesis Polymerization (ROMP)
- Should be stable in air and water with long shelf life
- Relatively inexpensive
- The monomer has to be compatible with the encapsulation method
- ROMP must be catalyzed by current catalytic system (Grubb's catalyst)
- The resulting polymerization must proceed rapidly over a wide temperature range
- The productivity [Turn Over Number (TON)] and the activity [Turn Over Frequency (TOF)] (discussed on next page) values for the new

monomer/catalyst system must be high so one can use an optimal monomer/initiator (M/I) ratio and minimize the catalyst cost.

The efficiency of new monomer was determined on the basis of Turn Over Number (TON) and Turn Over Frequency (TOF). These two terms are explained as follows.

1. Turn Over Number (TON): This is a productivity defined as grams of polymer formed per grams of catalyst (g polymer/g catalyst).

2. Turn Over Frequency (TOF): This is an activity defined as grams of polymer formed per grams of catalyst per unit of time [g polymer (g catalyst h)$^{-1}$].

Four commercial monomers were selected and compared with DCPD, as shown in Table 2.1.

Table 2.1 Comparison among different monomers

Sr. No.	Compound Name	Toxicity	Melting point (° C)	Boiling Point (° C)	Cost (CAD$/L)
1	Dicyclopentadiene (DCPD)	Flammable, environmentally hazardous, harmful	33 - 34	170	~70
2	5-ethylidene-2-norbornene (5E2N)	harmful	-80	146	~ 85
3	1,5-cyclooctadiene (COD)	harmful	-69	150	~ 75
4	Methylcyclopentadiene dimer (MCPD)	poisonous	-51	70 - 80	~ 60
5	5-vinyl-2-norbornene (5V2N)	harmful	-80	141	~ 160

The five compounds were compared based on the toxicity, melting point, boiling point and their costs. Among these five compounds, DCPD is harmful in addition to that it is

highly flammable and hazardous to the environment. 5E2N and 5V2N have almost same liquid temperature range but the cost of 5V2N is almost doubled than 5E2N. MCPD is poisonous with low boiling point.

ROMP tests were carried out with these monomers to check activity (TOF). For the experiments, 1 % w/w of Grubbs' catalyst was mixed with neat monomer with 500 rpm stirring rate at ambient atmosphere and at room temperature.

With these experimental conditions, the compound 5E2N underwent ROMP in less than 4 minutes while the COD, MCPD and 5V2N did not show proper polymerization with the Grubbs' catalyst. As such 5E2N was selected as a replacement to DCPD.

The next step was to perform more tests to study the kinetics of the 5E2N ROMP and determine the optimal conditions to be implemented in the final material and working temperature range. More tests were carried out to determine the activity of the 5E2N with catalyst. For these experiments 1 % w/w Grubbs' catalyst was used with neat 5E2N at 500 rpm stirring at ambient atmosphere and at -16, 0, 20, 45 °C. The polymerization times required to reach more than 90 % of monomer conversion and the corresponding activity at the temperatures for the 5E2N monomer are shown in Table 2.2 [27]. In this experiment 90 % of monomer conversion was an arbitrary decision on the end time, an apparent gel time formation.

Table 2.2 Polymerization time and activity of the 5E2N monomer as function of temperature [27]

Temperature (°C)	Activity (TOF) Kg polymer(Kg catalyst h)$^{-1}$	Polymerization time (min)
-16	0.46	146
0	1.7	40
20	20	3.5
45	320	0.2

Experimental conditions: Catalyst 1 % w/w, neat 5E2N with 500 rpm stirring at ambient atmosphere and at -16, 0, 20, 45 °C temperature

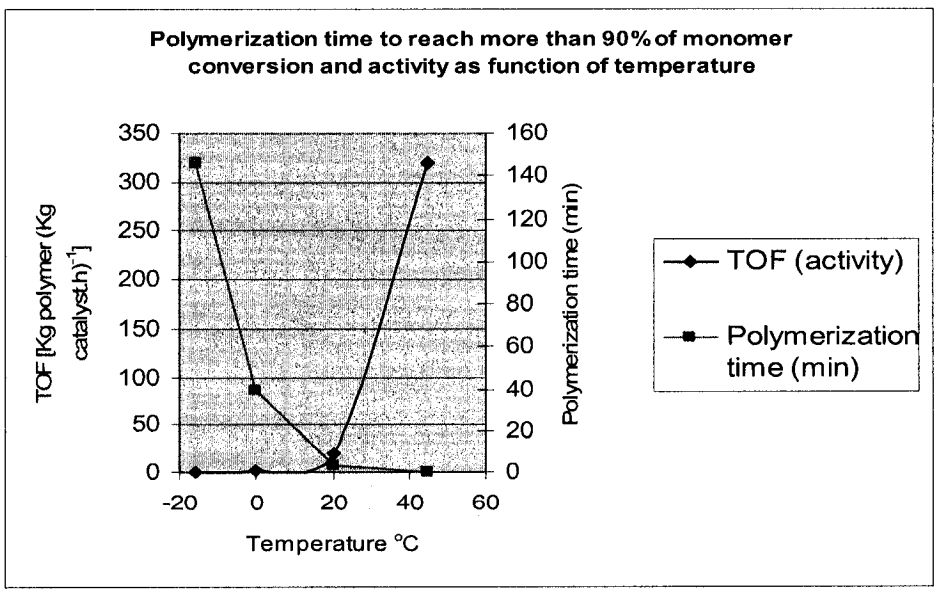

Figure 2.7 Graph of polymerization time and TOF (activity) as a function of temperature

Figure 2.7 shows that at 45 °C the polymerization duration is around 12 seconds and activity increases to 320 Kg polymer/Kg catalyst/h, whereas at -16 °C the polymerization duration is 2 hours and 26 minutes. Thus the temperature showed a strong influence on the system activity and curing kinetics.

Few experiments were carried out using different monomer/initiator (M/I) ratio and the productivity (TON) as function of M/I ratio was studied to find out optimal M/I ratio and reduce catalyst loading in the system. For these experiments neat 5E2N monomer and Grubbs' catalyst were used. The experiments were carried out at 20 °C in ambient atmosphere and 500 rpm stirring rate. Table 2.3 shows TON values for different values of M/I ratio.

Table 2.3 TON and TOF values for different values of M/I ratio using 5E2N [27]

M/I ratio	TON (mol polymer/mol Grubbs' catalyst)	TOF (mol polymer/mol Grubbs' catalyst/h)
9.80×10^3	9.60×10^3	1.6×10^5
1.30×10^4	1.30×10^4	2.0×10^5
2.00×10^4	1.90×10^4	2.5×10^5
2.40×10^4	2.30×10^4	2.7×10^5
2.80×10^4	2.70×10^4	2.9×10^5

Experimental conditions: Neat 5E2N, at 20 °C in ambient atmosphere, 500 rpm

Using Table 2.3, graph of TON (productivity) vs. different M/I ratios is plotted and shown in Figure 2.8.

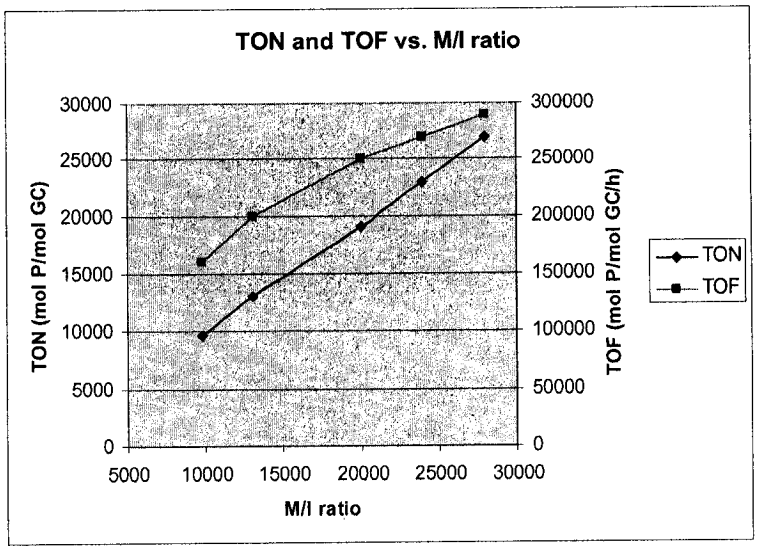

Figure 2.8 TON and TOF vs. M/I ratio graph for 5E2N ROMP at 20 °C

From Figure 2.8 it is clear that the higher is the M/I ratio (the w/w% of catalyst in system is reduced), the better is the TON (productivity). The TOF curve shows that the activity of the system is improved as M/I ratio increased. This is because for all five M/I ratios in this experiment, the polymerization time is almost same; varying from 3.5 to 5.5 min. This is advantageous as decrease in catalyst loading in the system did not show adverse effect on the activity of the system.

2.4 Microencapsulation

The microencapsulation process is a biphasic process: polymerization takes place at the surface of organic droplets suspended in an aqueous phase. The size of the capsules ranges from one micron to seven millimeters depending upon the stirring speed, the temperature, the system components and the agitator position and geometry [28].

Microencapsulation technique has many advantages such as encapsulation provides a way to protect the content from the deleterious effects of the surrounding environment or the reverse – thus toxic material can be safely handled. The delivery of compounds (e.g. a drug) can be controlled and even targeted. Another important advantage is that liquid can be handled as solid once encapsulated [28].

Due to many advantages, microencapsulation technique is widely used in the industries such as perfume industry, detergents industry, pharmaceuticals industry, adhesives industry etc [28, 29].

The shell of these microcapsules can be organic polymers, waxes and fats depending upon the envisaged application. The release of the core material from the capsule is usually achieved by the mechanical rupture of the capsule, diffusion through the shell, melting or dissolution of the shell or even ablation or biodegradation which means slow erosion of the shell [28].

The '*in situ* interfacial polymerization reaction' between urea and formaldehyde was used for the microencapsulation process. The reaction takes place at the interface between the aqueous phase and the second dispersed phase of the 5E2N monomer droplets. Figure 2.9 shows the schematic representation of the 5E2N microcapsule.

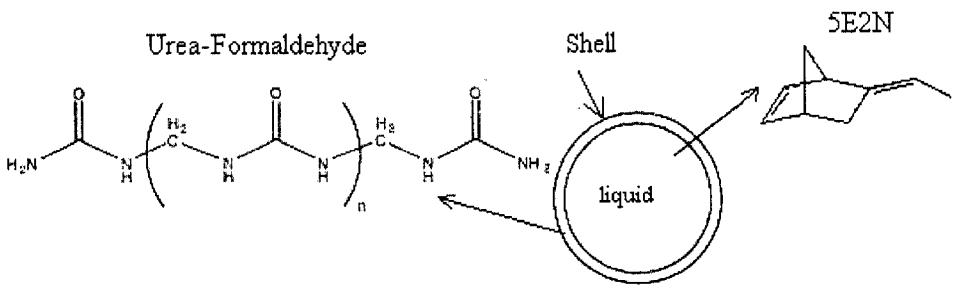

Figure 2.9 Schematic representation of a microcapsule

The microcapsule shell is produced during the step-growth polycondensation of urea and formaldehyde at the surface of the droplet of the organic shelf healing material. Figure 2.10 shows the step growth polymerization between urea and formaldehyde.

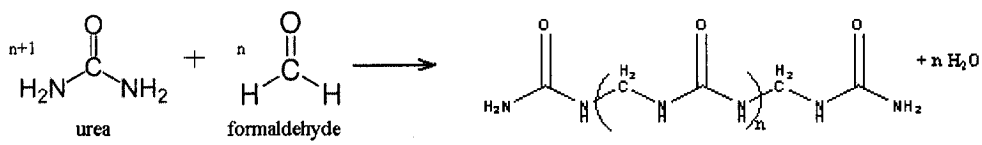

Figure 2.10 The step growth polymerization of urea and formaldehyde

2.5 Materials used for preparation of Microcapsules

As mentioned, the microcapsulation process is biphasic; the system components are the following:

Organic phase:-

- The self healing agent is 5-ethylidene-2-norbornene (5E2N); It is colorless at ambient temperature (b.p. = 146 °C) and is not miscible in water.

- Ethylene-Maleic-Anhydride (EMA) Copolymer is an odorless, solid soluble white powder, used as an organic emulsifier. It eases the formulation of a stable suspension of organic droplet in the aqueous phase.

Aqueous phase:-

- Urea is a white solid soluble in water. Formaldehyde is used here as a colorless 37 wt % aqueous solution.

- Resorcinol and ammonium chloride are both water soluble and serve as aqueous emulsifier and ease the polymerization process. 1-octanol is used to limit foaming.

- Hydrochloric acid and sodium hydroxide aqueous solution was used to adjust the pH of the solution to the correct value.

The materials 5E2N, urea, and resorcinol were obtained from Sigma-Aldrich®; the copolymer (EMA) was obtained from Zeeland Chemicals, USA and octanol and formaldehyde solution were obtained from the Fisher Scientific Company.

2.6 Experimental setup

The microencapsulation process requires a double jacket beaker to control the reaction temperature. A heater/chiller is coupled to control the circulation fluid temperature.

A mechanical stirrer driving a three-bladed low shear mixing propeller was placed inside the beaker. The rotation speed is inversely proportional to the size of the microcapsule produced. All the microencapsulation experiments were done in the CHEM lab in the Chemistry and Biochemistry department of Concordia University. The experimental set up is shown in the Figure 2.11.

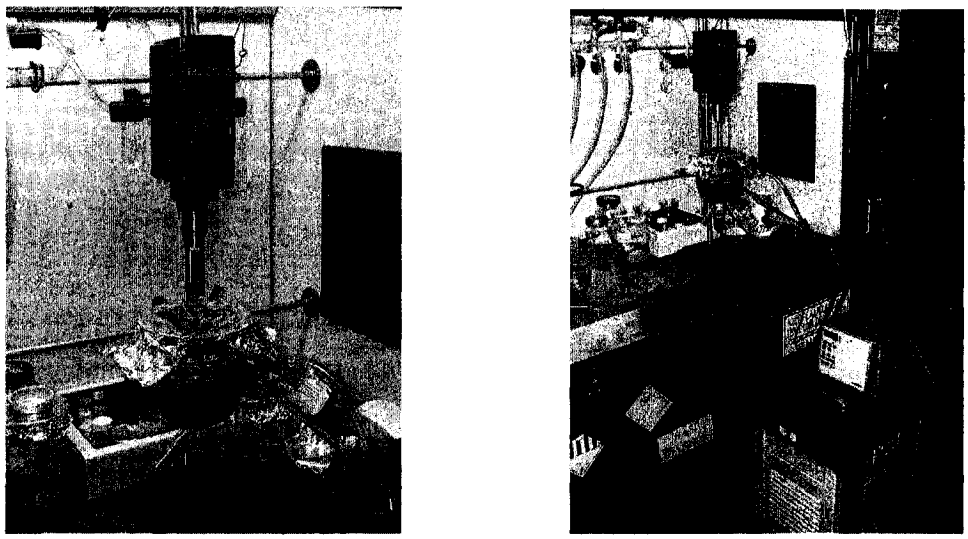

Figure 2.11 Experimental setup for the microencapsulation in the CHEM lab

2.7 Microencapsulation process

Three batches of microcapsules with different quantities of EMA solution were prepared and dried with different techniques to assure good quality of microcapsules. Table 2.4 summarizes three batches.

Table 2.4 Summary of different microencapsulation batches

Batch name	Monomer	Drying technique	Quantity of EMA solution(mL)
MC1	DCPD	Air	250
MC2	DCPD	New procedure	250
MC3	5E2N	New procedure	125

For the batches MC1 and MC2, urea (5 g), ammonium chloride (0.5 g), resorcinol (0.5 g) was dissolved in an EMA aqueous solution (250 mL, 0.5 %). An aqueous solution of formaldehyde (12.67 g, 37 %) was used. After air drying for 4 days the microcapsules showed agglomeration issue (Figure 2.12). Agglomeration of microcapsules is a problem and not desirable in self-healing system as it creates microcapsule rich/deficient area. This problem is solved as explained in section 2.8.

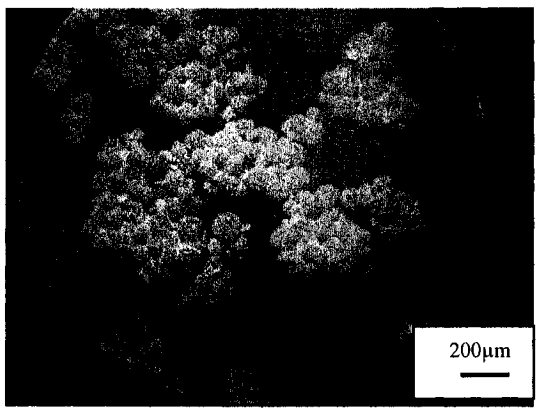

Figure 2.12 Agglomerated microcapsules (Batch MC1)

The microcapsules obtained from batch MC2 were dried with new technique as explained in section 2.8. The microcapsules obtained form this batch showed large particle size distribution from 90 - 400 μm as shown in Figure 2.13.

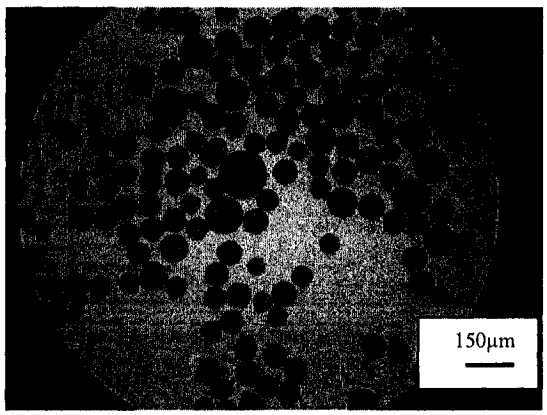

Figure 2.13 Microcapsules with wide variation in the diameter (Batch MC2)

2.8 New procedure to obtain good quality microcapsules

Modifications to the experimental protocol were made as explained below to solve the problem mentioned in section 2.7. It is important that the microcapsules have a relatively low particle size, uniform distribution and fulfill the free flowing requirement in order to achieve more homogeneous distribution of microcapsules within the matrix material.

The third batch (MC3) of 5E2N microencapsulation was carried out with the 125 mL EMA solution and all the other constituents were used accordingly. The detailed microencapsulation process is explained as follows.

Urea (2.25 g), ammonium chloride (0.25 g) and resorcinol (0.25 g) were dissolved in an EMA aqueous solution (125 mL, 0.5 %). The resulting solution was poured in a 1000 mL suspended double jacked reactor. The stirring speed was adjusted to 510 rpm. The pH of the solution was adjusted from 2.6 to 3.5 by drop-wise addition of aqueous sodium hydroxide (NaOH) and/or hydrochloric acid (HCl). One to two drops of 1-octanol were added to eliminate surface bubbles. Then, the 5E2N monomer (30 mL) was added slowly to form an emulsion and the solution obtained was allowed to stabilize for 10 minutes. An aqueous solution of formaldehyde (6.34 g, 37 wt %) was then added to the emulsion. The resulting white emulsion was covered and heated at a continuous rate to the target temperature of 55 °C during 4 hours and was then cooled at ambient temperature. A white solution was obtained with microcapsules in suspension.

After microencapsulation process the microcapsules were vacuum filtered and then rinsed with deionized water. Then the microcapsules were stored in deionised water for one day. Finally the microcapsules were dried under vacuum filtration. First microcapsules were washed with water, and then rinsed with acetone followed by ethyl ether under vacuum filtration and kept under vacuum for about 5 minutes.

The microcapsules were observed under the microscope. For this batch particle size diameter of the microcapsules were found to be from 150 - 350 μm. Figure 2.14 shows free flowing microcapsules from MC3 batch with less variation in the particle size diameter.

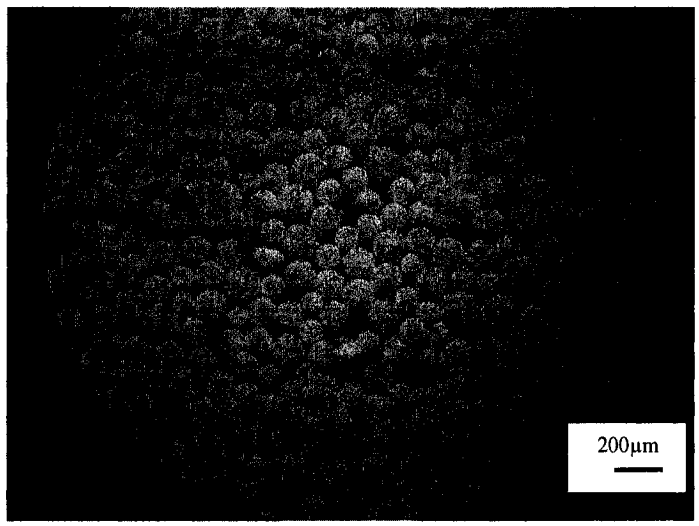

Figure 2.14 Free flowing microcapsules with less variation in particle size form MC3 batch

Figure 2.15 shows the white and spherical microcapsules with uniform and textured shell. This will optimize good bonding to the resin material and reduce slippage at the interface. We can thus expect that the microcapsule shell to break and to allow the healing material to flow in the crack.

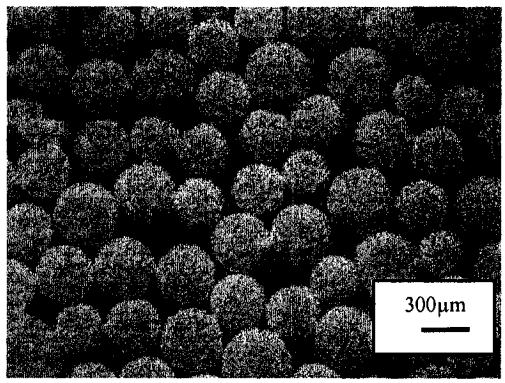

Figure 2.15 Textured surface of microcapsules

The microcapsule was ruptured by a pointed needle and free flow of 5E2N monomer outside the capsule shell was observed as expected (Figure 2.16).

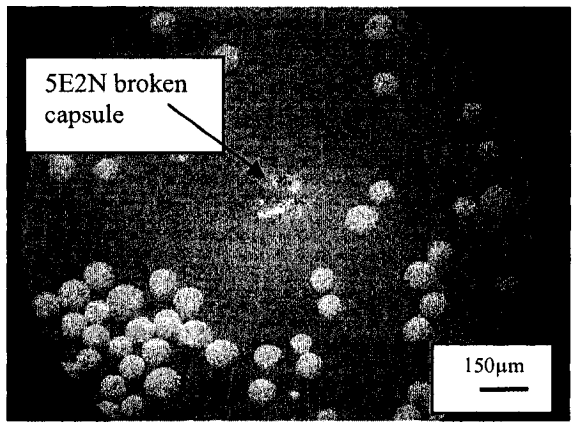

Figure 2.16 Free flowing of 5E2N monomer out of the microcapsule shell

Chapter 3

Sample preparation

Sample geometry, preparation of silicone mold and step by step procedure for preparation of sample for mechanical testing is explained.

3.1 Sample Geometry

As shown in Figure 3.1, standard Tapered Double Cantilever Beam (TDCB) geometry was used for sample preparation. Reason for selection of this geometry is explained in section 4.1.

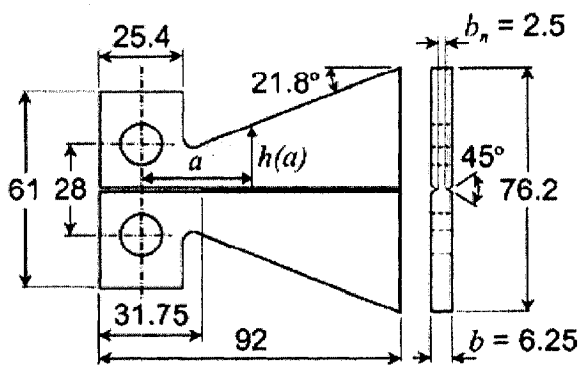

(All dimensions are in mm)

Figure 3.1 Tapered Double Cantilever Beam geometry [30]

3.2 Silicone rubber mold preparation

TDCB shaped aluminium pattern (Figure 3.2) was machined in the machine shop at Concordia University. A rectangular cardboard frame was fixed on the cleaned metal plate to form the mold cavity. 100 parts of Aircast 3700 silicone rubber was mixed with 15 parts of curing agent. These two compounds were mixed together for about 20 minutes to obtain a uniform mixture. These materials were obtained from MF Composites. Mixture was degassed in vacuum chamber for 30 minutes. Aluminium pattern was placed at the center of the mold cavity as shown in Figure 3.3. The degassed mixture was poured into the mold. The mold was cured at room temperature for 24 hours and at 50 °C for 24 hours. The fully cured silicone mold is shown in Figure 3.4.

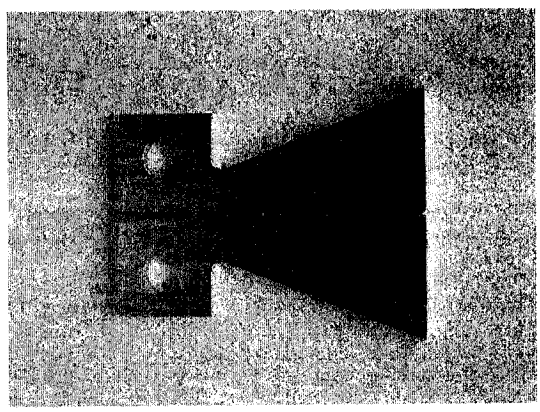

Figure 3.2 TDCB shaped aluminium pattern

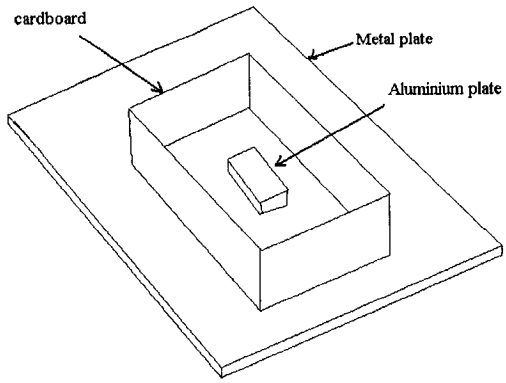

Figure 3.3 Setup for the preparation of silicone mold

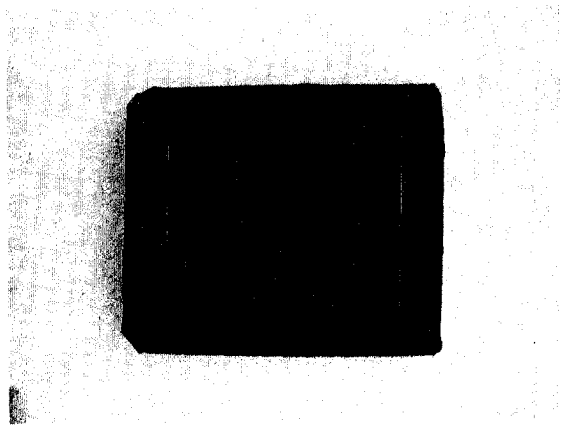

Figure 3.4 Fully cured silicone rubber mold

TDCB geometry has a notch on the both sides of the sample to ensure crack propagation at centerline of the sample. The silicone mold shown in Fig. 3.4 provides a notch on only one side of the sample. A schematic drawing of sample having notch on one side is shown in Figure 3.5.

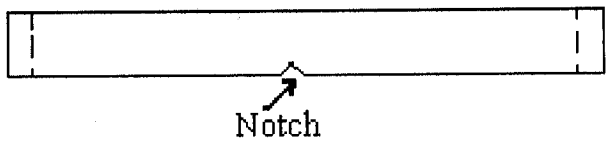

Figure 3.5 Sample with notch on one side

The neat samples (samples without microcapsules and catalyst) were prepared using the above mold. A blade notch was created to initiate the crack and the sample was loaded on MTS machine till failure. As shown in Figure 3.6 it was observed that the sample failed un-symmetrically.

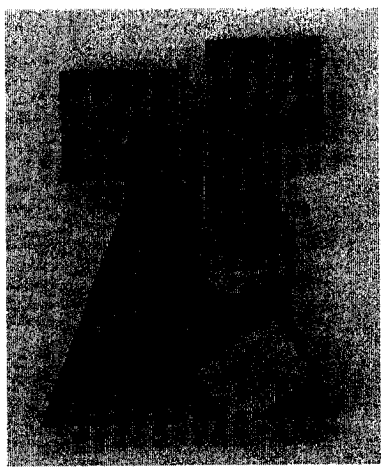

Figure 3.6 Neat sample failed un-symmetrically

To fulfill the requirements of the TDCB geometry and to ensure that the crack will propagate along the centre line of the sample; the sample must have notch on both faces as shown in Figure 3.7.

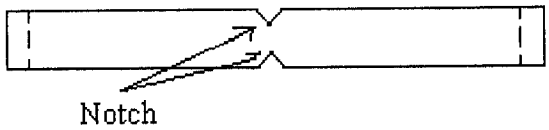

Figure 3.7 Sample with notch on both sides

Aluminium plate having notch shaped projection on one side at the centre line was machined (Figure 3.8). This plate acts in two ways, it provides a notch on the other face of the sample and also it acts as closure for the silicone mold. Figure 3.9 shows aluminium plate with notch shaped projection.

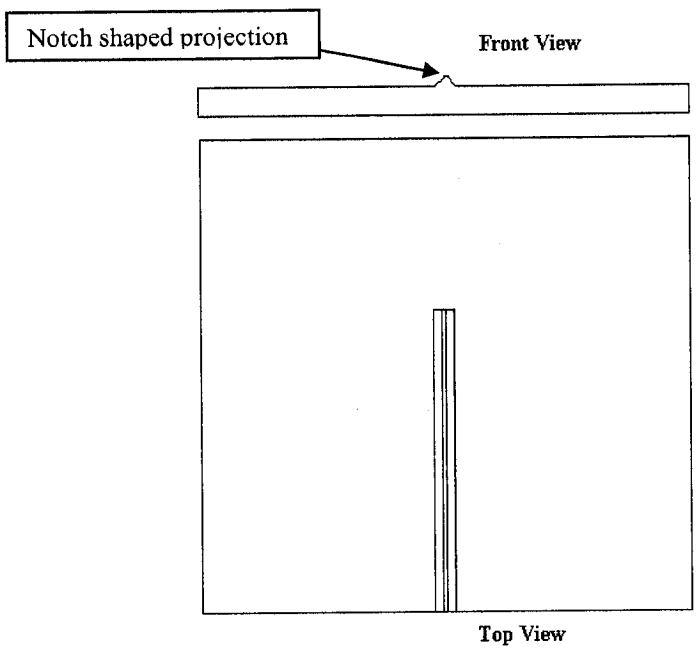

Figure 3.8 Schematic drawing of aluminium plate having notch shaped projection

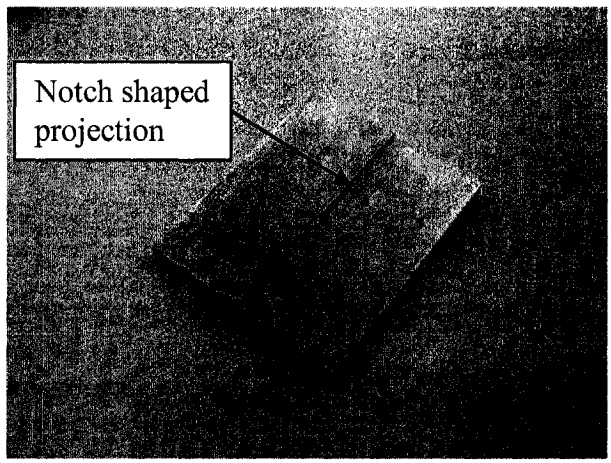

Figure 3.9 Aluminium plate with notch shaped projection

The neat sample with notch on both sides was tested on MTS machine. It was observed that, the sample failed symmetrically along the centerline as shown in Figure 3.10.

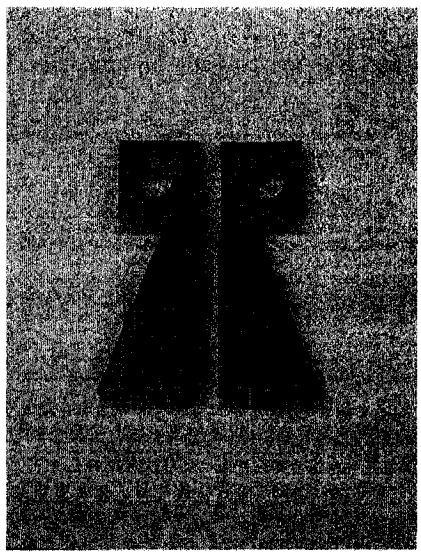

Figure 3.10 Neat sample failed symmetrically

3.3 Sample preparation

Two types of sample were prepared. Neat sample does not contain microcapsules and catalyst and another type was 5E2N sample; which contained microcapsules and catalyst. The sample preparation steps are discussed as follows.

a) Mixing:

Epon828 resin as matrix material and Epicure3046 as hardener were used for sample preparation. Both materials were obtained from Miller-Stephenson Chemical Co., Inc. The amount of hardener required for a specific quantity of resin was calculated using following formula.

$$H = \frac{E2}{E1} * 100 \quad \text{.....(1)}$$

Where,

H = amount of hardener required

$E1$ = Epoxy equivalent weight

$E2$ = Amine equivalent weight

The epoxy equivalent weight of Epon828 resin, $E1$ = 190 and amine equivalent weight of Epicure3046, $E2$ = 90. Using equation (1), for 100 parts of Epon828 resin; 47 parts of Epicure3046 was used.

For each sample, about 34 g of Epon828 and 16.1 g of Epicure3046 were mixed in a beaker for 15 minutes using a mechanical stirrer at a rate of 200 rpm. After proper mixing, the stirrer speed was adjusted to 150 rpm and slowly 10 % wt of microcapsules were added to the mixture. The stirring rate was lowered to avoid damage to the microcapsules. Then 1 % wt Grubbs' catalyst was added slowly to the mixture with continuous slow stirring rate. The mixture was kept agitated approximately for 10 minutes to obtain a homogeneous mixture. Then the mixture was degassed in vacuum chamber for 10 - 15 minutes to remove air bubbles. Then the mixture was poured into the silicone mold, covered with aluminium plate and kept for curing as shown in Figure 3.11.

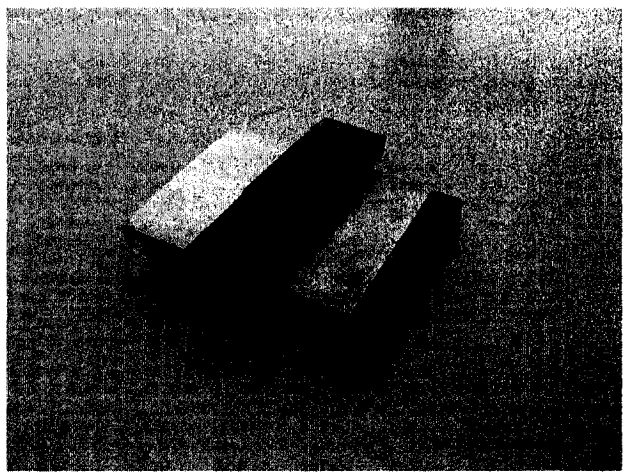

Figure 3.11 Silicone mold filled with the material and covered with aluminium plate

b) Curing cycle:

A Differential Scanning Calorimetry (DSC) test was done on the sample which was cured at room temperature for one day and at 45 °C for 2 days. DSC 2010 (TA Instruments) was used for this test. Figure 3.12 shows the DSC plot for the sample. The portion enclosed in rectangle does not show much exothermic reaction as a function of temperature which shows that the sample was almost cured. This curing cycle was used for all samples.

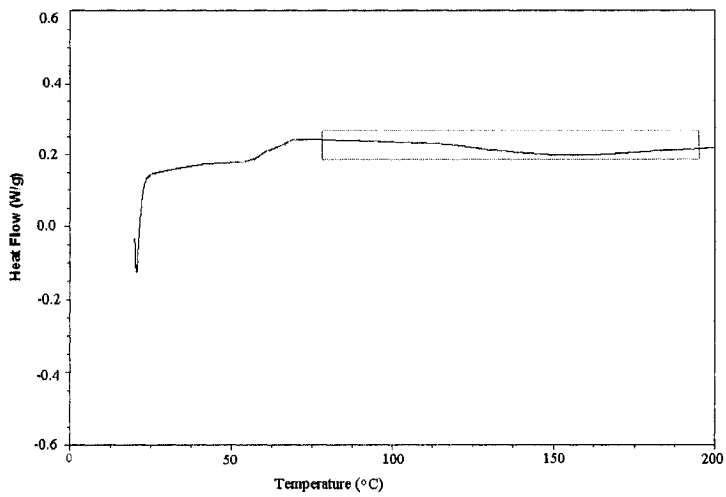

Figure 3.12 DSC plot for sample cured at room temperature for 24 hours and post cured at 45 °C for 48 hours

Figure 3.13 shows cured neat and 5E2N samples.

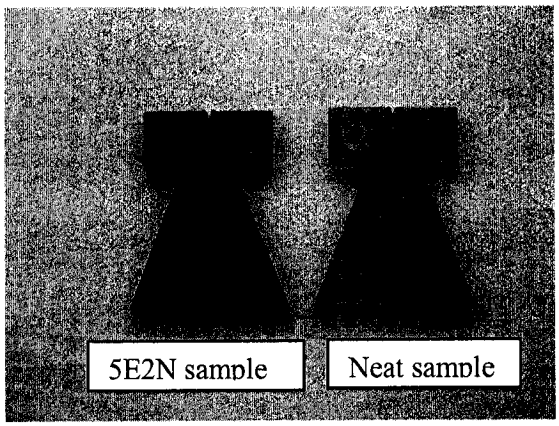

Figure 3.13 Cured 5E2N and neat samples

3.4 Microscopic observation of 5E2N samples

Sample containing 5E2N microcapsules and Grubbs' catalyst was observed under a Stereomicroscope. The microcapsules were observed to be in good condition in the sample without any damage as shown in Figure 3.14.

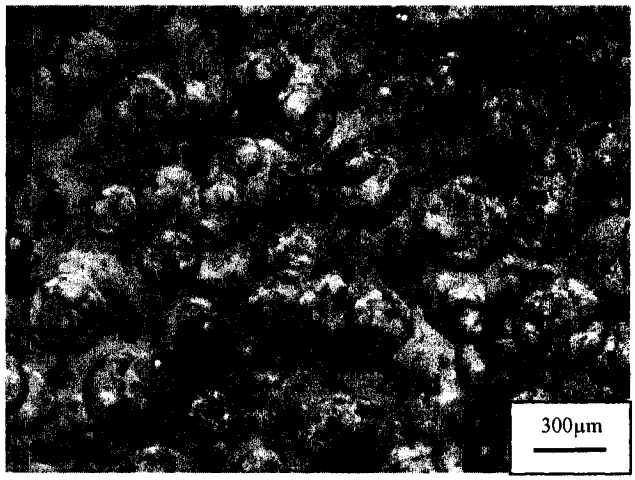

Figure 3.14 Condition of microcapsules in 5E2N sample

Condition of the monomer inside the sample was observed by breaking the microcapsule with the help of a syringe needle. As soon as the microcapsule was broken, it was observed that liquid monomer came out (Figure 3.15) and became solid due to polymerization reaction with Grubbs' catalyst (Figure 3.16).

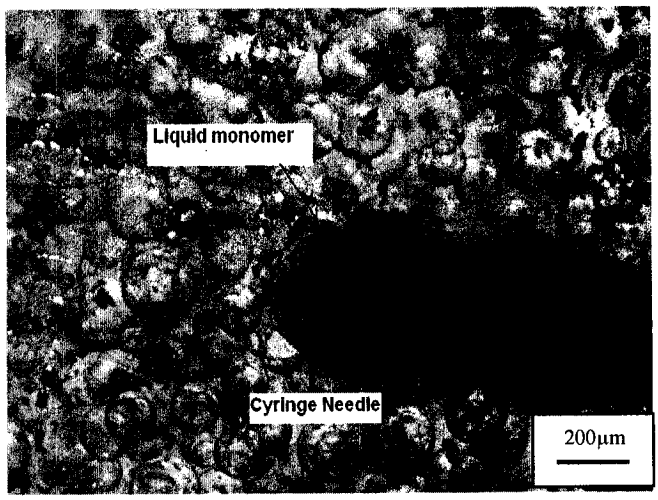

Figure 3.15 Liquid 5E2N monomer flowing out of the broken microcapsule

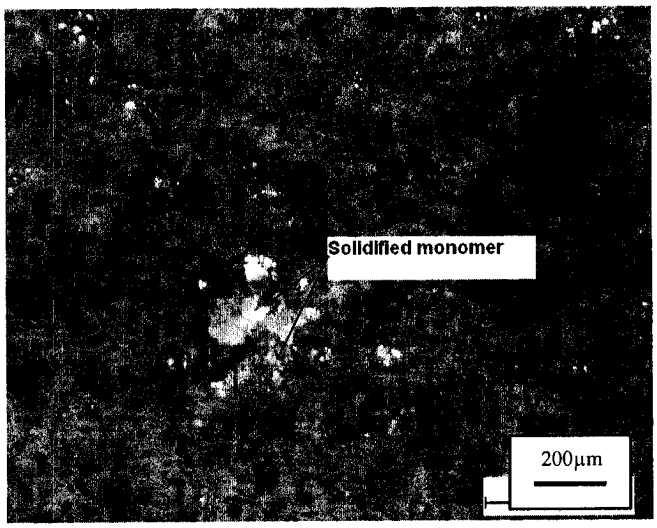

Figure 3.16 5E2N monomer flown out of the broken microcapsule and solidified due to polymerization

Chapter 4

Sample geometry and healing efficiency calculations

TDCB sample geometry is discussed and healing performance was determined with consideration of critical fracture of sample. The limitations of this approach were discussed and a new approach to determine healing performance is suggested here.

4.1 Sample geometry

For mechanical testing, Brown *et al.* used tapered double cantilever beam (TDCB) shaped samples as shown in Figure 4.1.

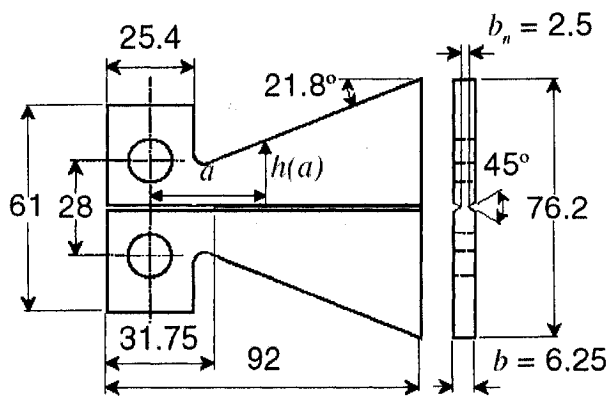

(All dimensions are in mm)

Figure 4.1 Tapered double cantilever beam (TDCB) geometry [30]

The samples were tested under displacement control of 5 μm/s using pin loading. The load vs. displacement graph for these samples was plotted as shown in Figure 4.2. The virgin curve represents the curve of a sample containing microcapsules and catalyst. A sharp pre-crack was created by gently tapping a razor blade in the molded starter notch and samples were tested to failure. These samples were allowed to heal for 48 hours and again tested to failure. The solid line graph in Figure 4.2 represents healed sample. Figure 4.2 shows that the virgin fracture was brittle in nature while healed fracture exhibited stick-slip phenomenon. The healing efficiency was calculated considering the critical fracture loads of the samples as explained later in this section.

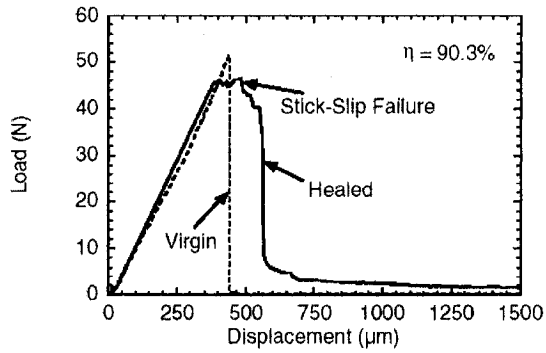

Figure 4.2 Load-displacement graph for virgin and healed sample [15]

The dimensions of TDCB sample shown in Figure 4.1 were obtained by Beres *et al.* from 2D, 3D finite element model and experimental results [31]. The benefits of this sample are presented later in this section.

Brown *et al.* defined healing efficiency as the ability of healed sample to recover fracture toughness. Equation (1) was used to calculate the healing efficiency [15].

$$\eta = \frac{K_{Ichealed}}{K_{Icvirgin}} \quad \text{.....(1)}$$

where, $K_{ICvirgin}$ is the fracture toughness of the virgin sample (samples without crack) and $K_{IChealed}$ is fracture toughness of the healed sample.

The crack extension force, G is defined as [32],

$$G = \frac{P^2}{2b_n}\frac{dC}{da} = (\text{N/mm}) \quad \text{.....(2)}$$

where, P is the applied load, b_n is the distance between notch tips, a is the crack length and C is the specimen compliance as function of crack length.

Mostovoy *et al.* [32] obtained an approximate analytic expression for the compliance C as a function of crack length by strength of material as given in equation (3)

$$C = \frac{24}{Eb}\int_0^a \frac{x^2}{h^3}dx + \frac{6(1+\nu)}{Eb}\int_0^a \frac{1}{h}dx \quad \text{.....(3)}$$

where, E is Young's modulus, ν is Poisson's ratio, b is the specimen width, x is the distance along the crack plane measured from the point of loading, h is the specimen height profile at the distance x.

The two terms on the right-hand side of the equation (3) are contributions to the compliance from bending and shear deflection, respectively.

For $\nu = 1/3$,

$$C = \frac{8}{Eb}\int_0^a \left(\frac{3x^2}{h^3} + \frac{1}{h}\right)dx \quad \text{.....(4)}$$

Integrating equation (4),

$$C = \frac{8}{Eb}\left(\frac{a^3}{h^3} + \frac{a}{h}\right) \quad \text{.....(5)}$$

Differentiating equation (5) with respect to a gives,

$$\frac{dC}{da} = \frac{8}{Eb}\left[\frac{3a^2}{h^3} + \frac{1}{h}\right] \quad \text{.....(6)}$$

Substituting equation (6) in equation (2) gives,

$$G = \frac{P^2}{2b_n} * \frac{8}{Eb}\left[\frac{3a^2}{h^3} + \frac{1}{h}\right] \quad \text{.....(7)}$$

or

$$G = \frac{4P^2}{\beta^2} * \frac{1}{E} m \quad \text{.....(8)}$$

where, $\beta^2 = b\ b_n$, (mm^2) and $m = \frac{3a^2}{h^3} + \frac{1}{h}$, (mm^{-1})

The relation between crack extension force G and fracture toughness K_{IC} is given as [33],

$$K_{IC}^2 = G * E \quad \text{.....(9)}$$

Substituting Eq (8) in Eq (9) and taking square-root yields,

$$K_{IC} = 2P \frac{\sqrt{m}}{\beta} \quad \text{.....(10)}$$

where m and β are the geometric terms. The value of β depends on the specimen width 'b' and the distance between crack tip 'b_n'. For the geometry shown in Fig. 4.1, β is given by [15, 34]

$$\beta = b^{0.61} b_n^{\ 0.39} \quad \text{.....(11)}$$

From Figure 4.1, $b = 6.25$ mm and $b_n = 2.5$ mm,

$$\beta = 4.371 \text{ mm}$$

The simple trigonometric calculations were performed to determine the effect of crack length on the values of m, where m is given by Eq (12)

$$m = \frac{3a^2}{h(a)^3} + \frac{1}{h(a)} \quad \text{.....(12)}$$

Equation (12) is simplified and converted to an equation in terms of 'a' only. Specimen height profile 'h' is a function of a and using trigonometry 'h' can be written in terms of 'a'.

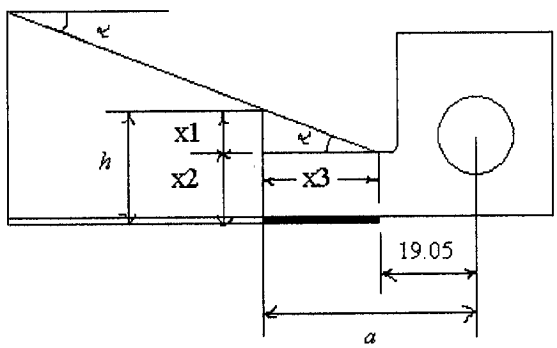

Figure 4.3 Schematic diagram of half portion of TDCB with dimensions

In Figure 4.3, $\alpha = 21.8^{o}$, a is the crack length (mm), h (mm) = x1 + x2. The values of x1, x2 and x3 were obtained from Figures 4.1 and 4.3.

x1 = tan 21.8 * x3, mm

x2 = 14 mm

x3 = (a - 19.05), mm

Using values of x1, x2 and x3, h can be calculated as follows

$$h = 6.57 + 0.39\,a \quad \text{.....(13)}$$

Substituting equation (13) in equation (12), 'm' can be written as

$$m = \frac{3a^2}{(6.57 + 0.39a)^3} + \frac{1}{(6.57 + 0.39a)} \quad \text{.....(14)}$$

From Eq (14), the values of m were determined for different values of crack length 'a' (Table 4.1).

Table 4.1 Different values of 'm' for different crack length 'a'

Sr. No.	Crack Length 'a' (mm)	m (mm^{-1})
1	20	0.47
2	22	0.48
3	24	0.48
4	26	0.49
5	28	0.49
6	30	0.49
7	32	0.49

Table 4.1 shows that the values of 'm' is almost constant for different values of crack length 'a'. The value of $\beta = 4.371$, is also constant. As a result the fracture toughness represented by equation (10) only depends upon applied load P. As such equation (1) became,

$$\eta = \frac{P_{Chealed}}{P_{Cvirgin}} \quad \text{.....(15)}$$

4.2 Calculation of healing efficiency

The same approach used by Brown *et al.* was used to calculate the healing efficiency. The critical fracture loads of samples were considered and the healing efficiency was calculated using Eq (15). The experimental data as explained in section 5.3, for neat and 5E2N samples without sharp crack and for neat and 5E2N samples conditioned at 23 °C were selected.

The load vs. displacement graph for neat and 5E2N samples without sharp crack is shown in Figure 4.4. Figure 4.4 shows brittle failure of the both types of samples and curves clearly show that the addition of microcapsules and catalyst lowered the critical fracture load and stiffness of the samples.

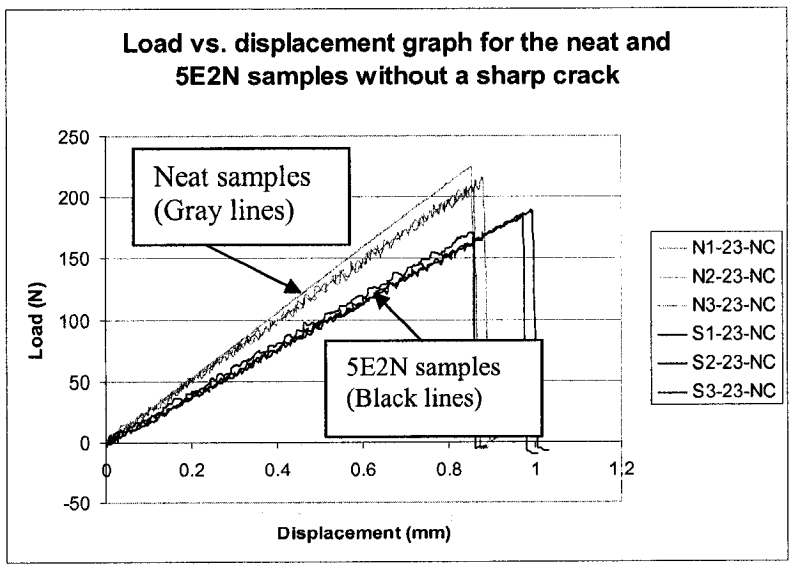

Figure 4.4 Load vs. displacement graph for neat and 5E2N samples without sharp crack

Summary of results of neat and 5E2N samples without sharp crack are shown in the Tables 4.2 and 4.3 respectively.

Table 4.2 Summary of results of neat sample without a sharp crack

Sr. No.	Sample name	Maximum Load (N)	Stiffness (N/mm)
1	N2-23-NC	208	215
2	N1-23-NC	225	265
3	N3-23-NC	214	220
Average		$P_1 = 215.6$	$S_1 = 233$

From Table 4.2, the average critical fracture load of the three neat samples is 215.6 N and average stiffness of these three samples is 233 N/mm.

Table 4.3 Summary of results of 5E2N samples without a sharp crack

Sr. No.	Sample name	Maximum Load (N)	Stiffness (N/mm)
1	S1-23-NC	170	205
2	S2-23-NC	188	192
3	S3-23-NC	184	193
Average		$P_2 = 180.6$	$S_2 = 196$

From Table 4.3, average critical fracture load and stiffness of the three 5E2N samples is 180.6 N and 196 N/mm respectively.

The critical fracture load and stiffness values from Tables 4.2 and 4.3 shows that addition of microcapsules and catalyst to the neat sample lowered the average critical fracture load by 16 % and stiffness by 15.8 %. Considering this fact, the neat sample was considered as reference sample instead of 5E2N sample. This approach to determine the healing efficiency will consider the effect of addition of microcapsules and catalyst to samples on material properties.

Figure 4.5 shows enlarged view of the initial portion of load vs. displacement graph for the neat and 5E2N samples with a sharp crack and conditioned at 23 °C.

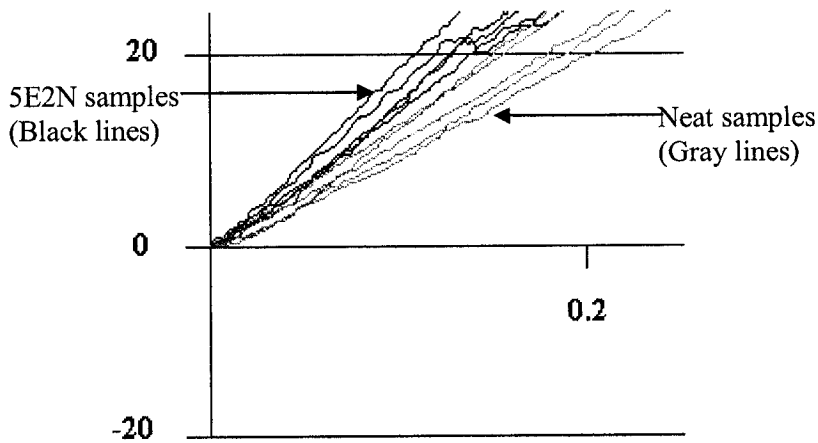

Figure 4.5 Enlarged view of initial portion of load vs. displacement graph for neat and 5E2N samples with a sharp crack, conditioned at 23 °C

Tables 4.4 and 4.5 show the summary of the results of neat and 5E2N samples with sharp crack, conditioned at 23 °C for one day for healing purpose.

Table 4.4 Summary of results of neat samples with a sharp crack and conditioned at 23 °C for one day

Sr. No.	Sample name	Crack length (mm)	Critical fracture load (N)
1	N4-23-WC	23	84
2	N5-23-WC	26	91
3	N6-23-WC	32	91
4	N8-23-WC	28	84
5	N9-23-WC	36	58
Average critical fracture load $P_3 = 81.6$ N			

Table 4.5 Summary of results of 5E2N samples with a sharp crack and conditioned at 23 °C for one day

Sr. No.	Sample name	Crack length (mm)	Critical fracture load (N)
1	S4-23-WC	23	68
2	S6-23-WC	23	99
3	S7-23-WC	32	82
4	S8-23-WC	27	75
5	S9-23-WC	24	80
Average critical fracture load $P_4 = 80.8$ N			

From Tables 4.4 and 4.5 the average critical fracture load of neat and 5E2N samples with sharp crack are 81.6 and 80.8 N respectively.

From Tables 4.4 and 4.5 it is clearly shown that the majority of the neat samples have greater critical fracture load than the 5E2N samples. Equation (15) is used and the ratios, P_3/P_1= 81.6/215.6 = 37.8 % and P_4/P_1 = 80.8/215.6 = 37.4 % were calculated. However from Figure 4.5 the slope of the curves shows that the 5E2N samples are stiffer than the neat samples. The comparison between the load values may not give a good indication of the healing performance. This is explained in more detailed as follows.

TDCB specimen provides the crack length independent measure of fracture toughness. This is based solely on the geometric conditions. In equation (3), the compliance C has an expression for bending and another for shear based on modulus and geometry. This does not take in to consideration the crack tip geometry, material at the tip of the crack and crack arrest phenomenon which have major effect on the critical fracture load.

If the material at the tip of crack is stronger then the maximum load required to fracture the sample would be higher. The same thing effect goes with the effect of curvature at the tip of the crack.

The equivalency between equation (1) and (15) will only hold if all geometric parameters are the same and the materials at the crack tip are the same between virgin sample and healed sample. However in reality, it is difficult to keep them the same, particularly where the presence of microcapsules and catalyst would alter the properties of the virgin materials and the binding effect of healing would alter the curvature at the crack tip.

Considering the fact that a healed crack would become a shorter crack, the use of stiffness (or slope of the load/deflection curve) would be a better way to represent the efficiency of healing. This can be shown in Figure 4.6.

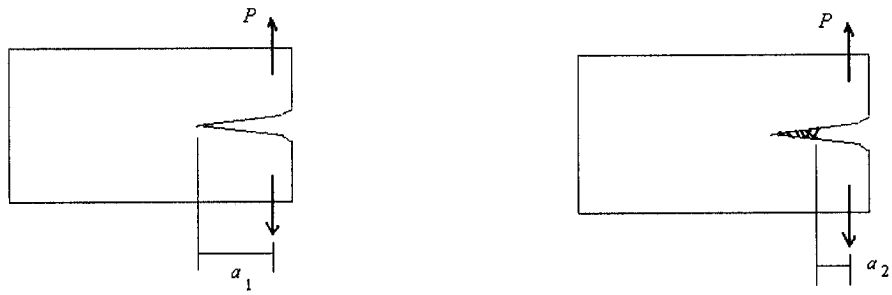

(a) (b)

Figure 4.6 Sample with different crack length (a) Initial crack length a_1, (b) healed sample with reduced crack length a_2

In Figure 4.6, crack is of length a_1. Due to healing, the crack length is effectively reduced to $a_2 < a_1$. If load is applied (b) sample would show a larger stiffness (larger slope of the curve) than the (a) sample. Using stiffness as an indication of healing efficiency provides a method that is independent of the crack tip geometry or properties of material at the crack tip may be good choice.

For the use of stiffness as an indication of healing efficiency, the following definitions are used.

The four different cases of samples with different materials composition and with and with out sharp crack were considered.

Case 1: Consider neat sample. This sample does not contain any microcapsules and catalyst. Assume that its critical fracture load and stiffness are P_1 and S_1 respectively.

Case 2: Consider another type of sample containing microcapsules and catalyst. Assume that the critical fracture load and stiffness are P_2 and S_2 respectively. Since the specimen now contains soft particles and catalyst, the stiffness and strength of the material are less than that of neat sample.

Case 3: Neat sample with crack of length a is considered. Assume that P_3 is the critical fracture load of this sample.

Case 4: Sample containing microcapsules and catalyst with crack of length a is considered. This sample is allowed to heal for one day. Assume that due to healing of crack, crack length is reduced from a to a_1. P_4 is the critical fracture load of this sample.

Schematic representation of all above four cases is shown in Figure 4.7.

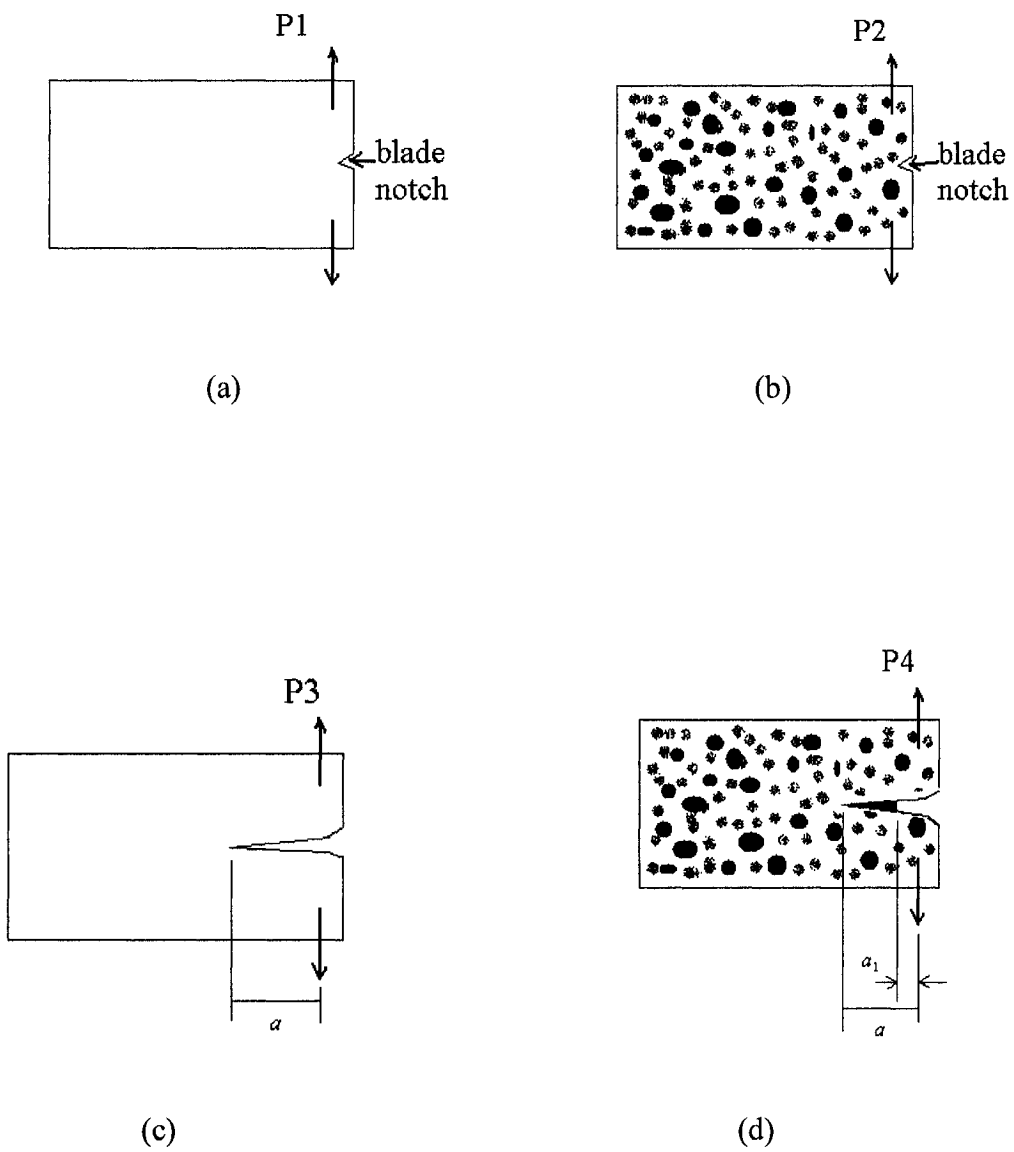

Figure 4.7 Schematic representation of (a) case 1, (b) case 2, (c) case 3 and (d) case 4

Load vs. displacement plots for all four cases was made as shown in Figure 4.8. P_1, P_2, P_3, P_4 and S_1, S_2, S_3 and S_4 are the critical fracture load and stiffness of case 1, case 2, case 3, case 4 respectively.

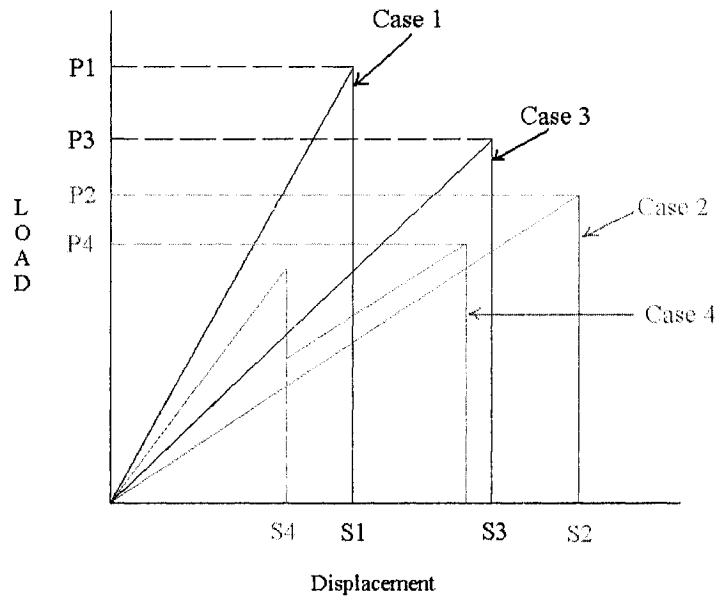

Figure 4.8 Schematic representation of load vs. displacement for case 1, case 2, case 3 and case 4

Assume that, case 1 showed maximum critical fracture load and stiffness as it does not have crack and any soft particles. Addition of microcapsules and catalyst to material lowered the modulus and as such $P_2 < P_1$ and $S_2 < S_1$. In presence of crack the critical fracture load of neat sample (case 3) P_3 should be less than P_1. The critical fracture load P_4 may be more or less than P_3 depending upon crack tip geometry and crack arrest phenomenon.

4.3 New approach to determine healing efficiency

As discussed in section 4.2, consideration of critical fracture load of a sample to determine healing efficiency may not be an accurate way. This necessitates implementation of new approach to determine the healing performance.

New approach to determine the healing performance is proposed. Stiffness which is a ratio of load and displacement was considered for the determination of healing performance (Figure 4.9).

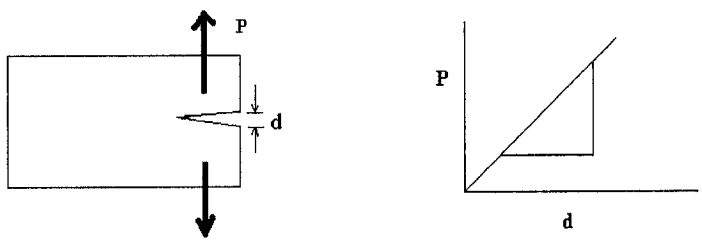

Figure 4.9 Load vs. displacement graph for sample subjected to tensile loading

From figure 4.9 stiffness value can be determined as,

$$Stiffness = \frac{\Delta P}{\Delta d} \quad \text{.....(16)}$$

Case 3 and Case 4 from section 4.2 are considered. Neat sample with crack length a, subjected to tensile load P, assume that the crack opening displacement is d_1 (Fig.4.10).

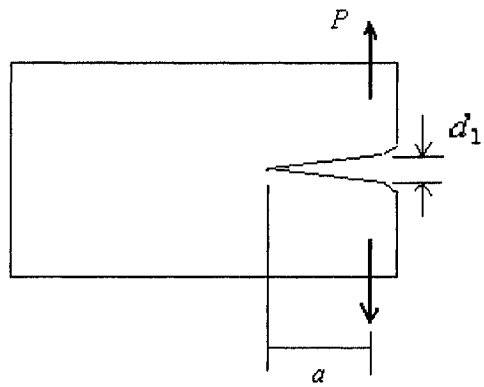

Figure 4.10 Schematic diagram representing neat sample with crack length a and crack opening displacement d_1

From the stiffness definition, the stiffness S_3 of the neat sample is given by the Eq 17.

$$S_3 = \frac{P}{d_1} \quad \ldots\ldots\ldots\ldots\ldots\ldots\ldots\ldots\ldots (17)$$

Sample in case 4, due to healing process the healing material in the crack plane acts as bonding material to keep the two crack faces together and it will reduce the crack length from a to a_1. Assume that for the tensile load P, the crack opening displacement is d_2 (Fig. 4.11) which is less than d_1, as healing material resist opening the crack.

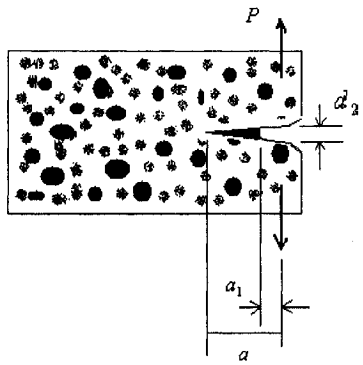

Figure 4.11 Schematic diagram representing healed 5E2N sample with crack length a_1 and crack opening displacement d_2

The stiffness of this sample is given by

$$S_4 = \frac{P}{d_2} \quad \text{..... (18)}$$

The portion of load-displacement graph as shown in rectangle in Figure 4.12 is used to determine the stiffness S_4 and S_3. In case 4, the healing material in the crack bonds the two crack faces and resist for the crack opening. On contrary to this the neat sample with no healing material in crack will show the more crack opening displacement. As such S_4 may be more than S_3.

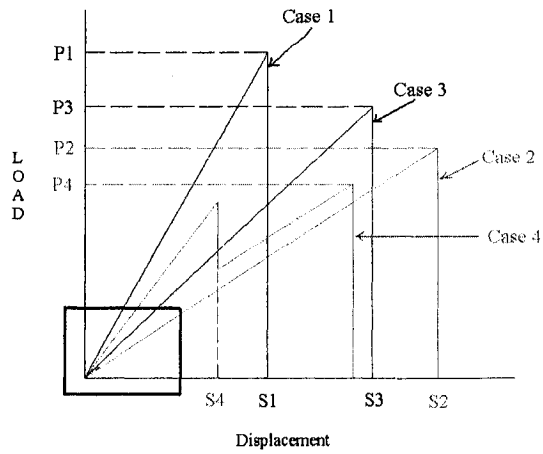

Figure 4.12 Portion shown in rectangle is the portion of interest to determine the stiffness values of the samples

These two stiffness values were compared with S_1 (Case 1). The ratio S_3/S_1 will give percentage stiffness of neat sample in presence of sharp crack and the ratio S_4/S_1 will give percentage stiffness of healed sample in presence of a sharp crack. This approach will be used in chapter 5 to determine the healing efficiency of the samples. Also the same approach discussed in section 4.1 related to Figure 4.2 was considered and the ratio of critical fracture loads P_4/P_3 is discussed in chapter 5. The difference here is that the virgin sample (critical fracture load P_3) represents neat sample with initial sharp crack contrary to the virgin sample discussed in Figure 4.2. This difference considers the effect of addition of microcapsules and catalyst on the material properties while calculating healing efficiency.

Chapter 5

Environmental Conditioning, mechanical tests and results

5.1 Environmental Conditioning

Space environment has a wide temperature range from -156 °C to +121°C [35]. Along with this, space has some special aspects such as high vacuum, UV radiation, atomic Oxygen etc. The effect of some of these factors and effect of different temperatures on the healing performance was studied. The different environmental conditioning tests were carried out as explained below,

1. Different temperature tests: The effect of different temperatures on the healing performance was studied. Tests have been carried out at 23, 45, 60, 100 °C at Concordia University Composites lab. Samples were conditioned at different temperatures using the oven.

2. Healing performance was tested at -20 °C. This test was carried out in an environmental chamber at MBP Technologies Inc. Samples with a sharp crack were placed in the environmental chamber maintained at -20 °C for 24 hours. Figure 5.1 shows the environmental chamber used for this test.

Figure 5.1 Environnemental chambre (MPB Technologies Inc.)

3. Vacuum tests: These tests were carried out at $10^{-6} mbar$ of vacuum. The vacuum test was done at two different temperatures, one at 23 °C (room temperature) and another at 80 °C. Figure 5.2 shows vacuum chamber used for this test.

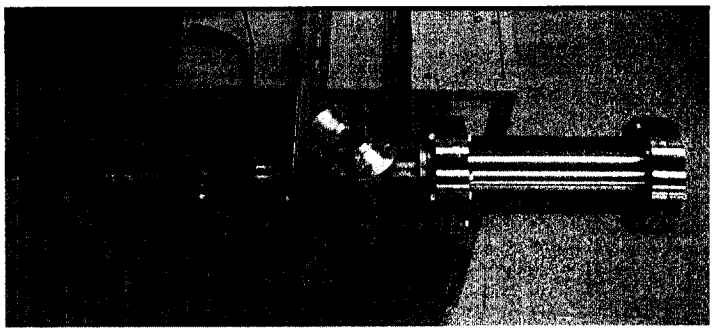

Figure 5.2 Vacuum chamber (MPB Technologies Inc.)

Vacuum test at 80 °C was done using a special heating arrangement. Heating foils were used. Aluminium plates were used to support heating foils. Figure 5.3 show schematic heating arrangement. Samples with sharp crack were put

into the vacuum chamber at $10^{-6} mbar$ and temperature of the heating foil was maintained 80 °C. Samples were kept in vacuum for 24 hours. Figure 5.4 shows the heating setup arrangement for the samples.

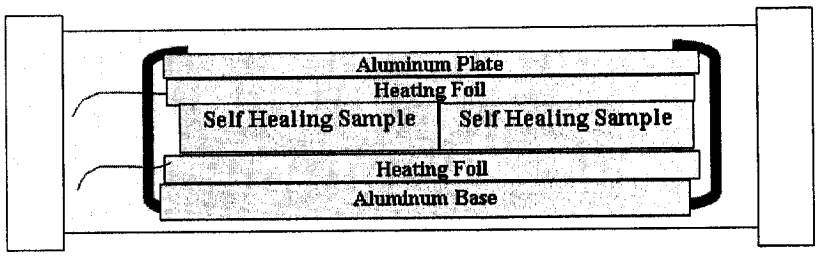

Figure 5.3 Schematic diagram of heating arrangement for samples in vacuum chamber

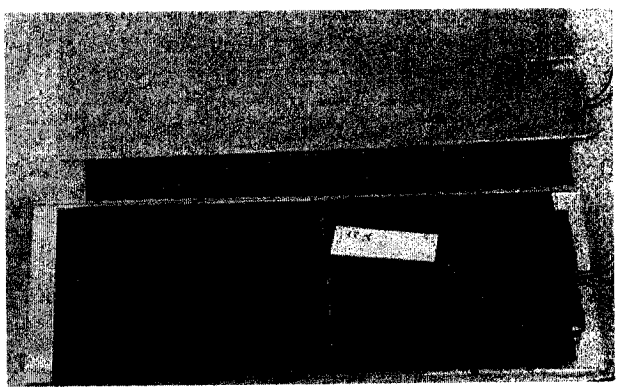

Figure 5.4 Heating setup used for heating the samples in vacuum chamber

4. Thermal shock test: This test was carried out to determine the effect of temperature fluctuation on healing performance.

   This test was carried out by subjecting the two types of samples to cooling-heating cycle. Liquid nitrogen was used for cooling purpose (boiling point = -196 °C) and samples were heated in an oven at 60 °C. Samples were kept for 5 min in liquid nitrogen and transferred to the oven temperature in less than one minute and left it for 5 minutes in oven.

5. Young's modulus of the healing material was determined. As shown in Figure 5.5, four bone shaped samples were prepared using the 5E2N monomer and 1 % Grubbs' catalyst. The simple tensile tests were carried out on MTS machine.

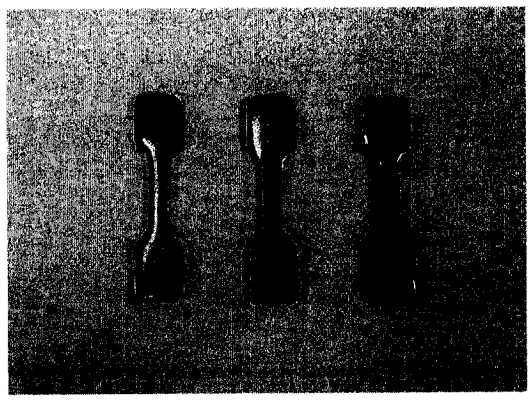

Figure 5.5 Bone shaped monomer samples (5E2N + 1 % Grubbs catalyst')

5.2 Mechanical test procedure

Samples conditioned for healing for one day were tested on MTS (300 KN) machine with load cell of 2.5 KN. As shown in Figure 5.6, samples were pin loaded on MTS machine and tensile load was applied under displacement control using 5 μm/s displacement rate.

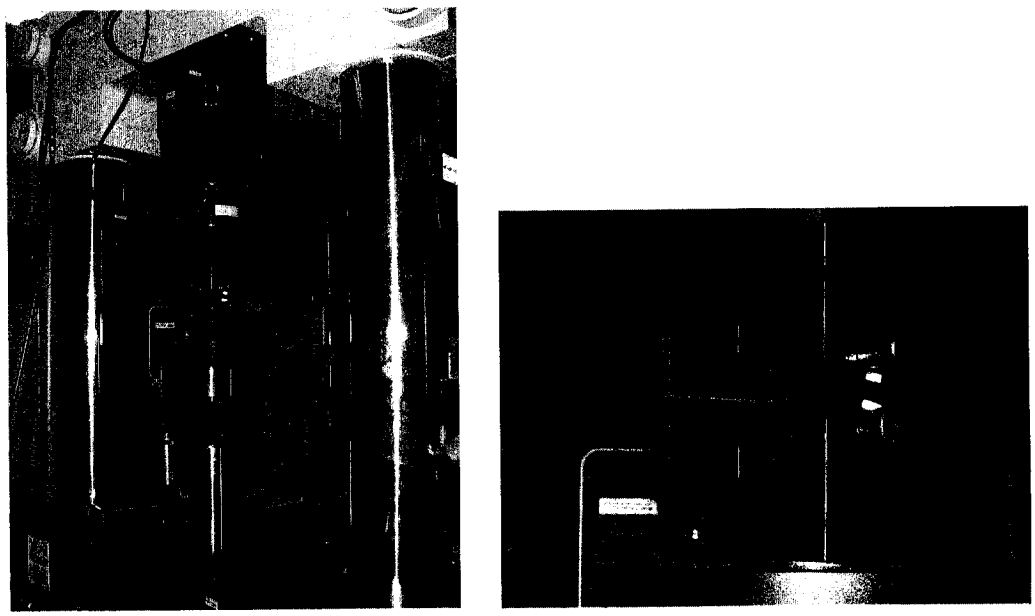

(a) (b)

Figure 5.6 (a) MTS machine (300 KN), (b) pin loaded sample on MTS machine

Before going to actual testing procedure the sample types and their conditions are discussed. As shown in Figure 5.7 two main types of sample named neat (sample with no microcapsules and catalyst) and 5E2N (samples containing microcapsules and Grubbs' catalyst) samples were tested. Each type of sample was divided in to two sub sets as one

set of samples without sharp crack and another set of samples with sharp crack. The set of samples with sharp crack was tested after one day of conditioning in desired environment.

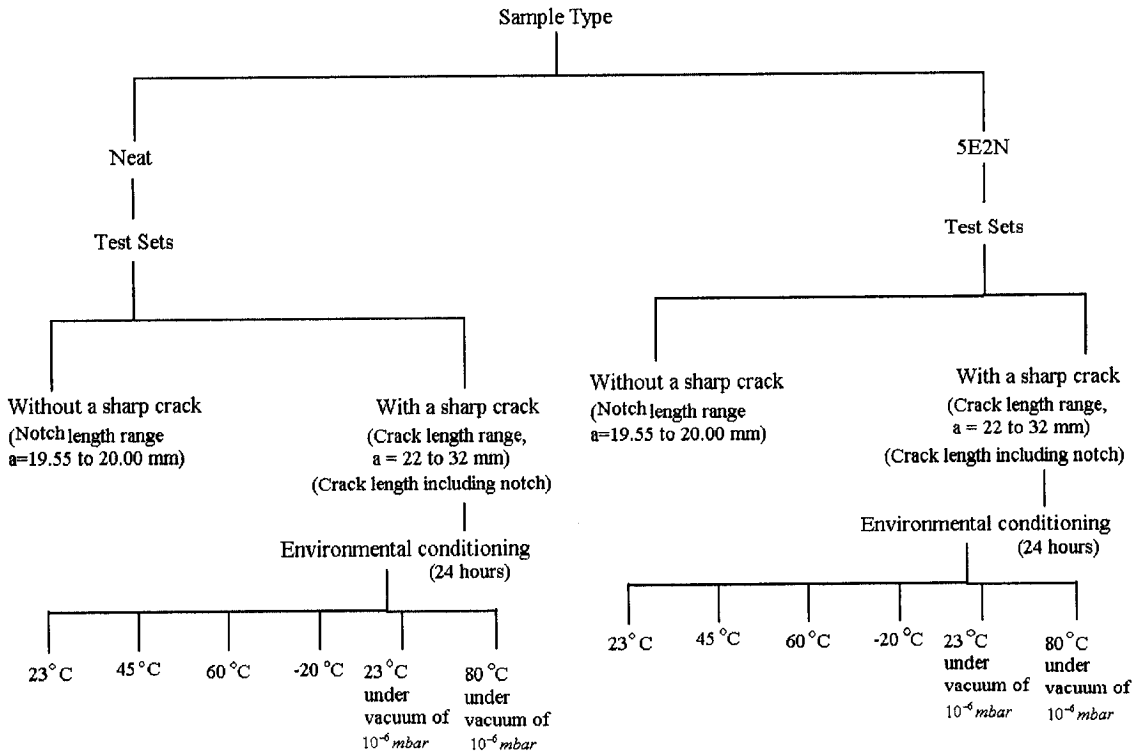

Figure 5.7 Tree diagram showing different types of samples and different conditions

Step by step testing procedure is described as follows.

1. Samples without a sharp crack: The neat and 5E2N samples with a blade indentation at notch tip were pin loaded on MTS machine and tensile load was applied till failure. Load vs. displacement plots were made. Figure 5.8 shows sample with an indentation at a notch tip.

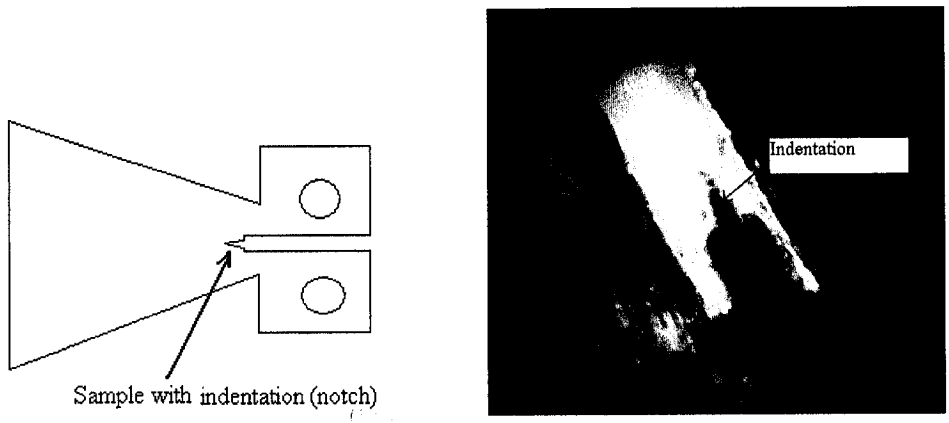

Figure 5.8 Sample with a blade indentation at a notch tip

2. Samples with a sharp crack: The neat and 5E2N samples with a sharp crack at indentation tip were considered. These sets of samples were tested in two steps. First a sharp crack was produced with the help of blade and hammer (Figure 5.9). Then the samples were kept at desired environmental condition for one day to ensure full healing of crack plane. After 24 hours the samples were tested on MTS machine till failure. Load vs. displacement plot were made.

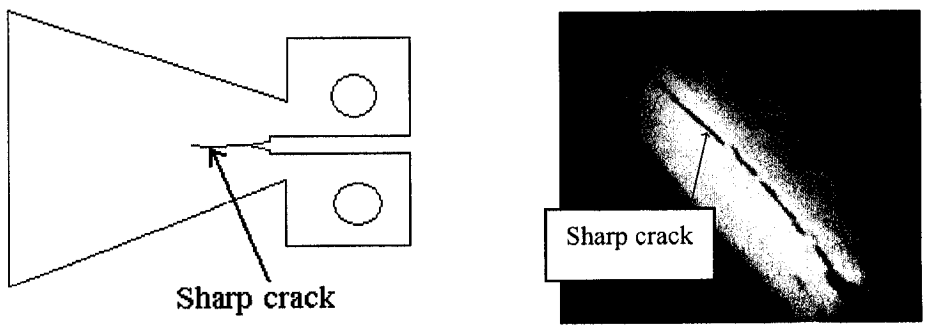

Figure 5.9 Sample with a sharp crack

All the neat and 5E2N samples tested at different environmental conditions are summarized in the Table 5.1 and 5.2 respectively. An abbreviation was sequenced as first letter and number indicated as sample type and sample number respectively, followed by the environmental condition and the last two letters are for the presence of the crack. For example N1-23-NC means neat sample-1 conditioned at 23 °C with no sharp crack and S26-V23-WC means 5E2N sample-26 with sharp crack and conditioned at 23 °C under vacuum.

Table 5.1 Summary of all neat samples

Sr. No	Sample name	Environmental Conditions	Presence of crack	Abbreviation
1	Neat-1	23	No	N1-23-NC
2	Neat-2	23	No	N2-23-NC
3	Neat-3	23	No	N3-23-NC
4	Neat-4	23	Yes	N4-23-WC
5	Neat-5	23	Yes	N5-23-WC
6	Neat-6	23	Yes	N6-23-WC
7	Neat-8	23	Yes	N8-23-WC
8	Neat-9	23	Yes	N9-23-WC
9	Neat-10	45	Yes	N10-45-WC
10	Neat-11	45	Yes	N11-45-WC
11	Neat-12	45	Yes	N12-45-WC
12	Neat-13	45	Yes	N13-45-WC
13	Neat-14	45	Yes	N14-45-WC
14				
	Neat-15	60	Yes	N15-60-WC
15	Neat-16	60	Yes	N16-60-WC
16	Neat-17	60	Yes	N17-60-WC
17	Neat-18	60	Yes	N18-60-WC
18	Neat-19	60	Yes	N19-60-WC
19	Neat-20	-20	Yes	N20-(-20)-WC
20	Neat-21	-20	Yes	N21-(-20)-WC
21	Neat-22	-20	Yes	N22-(-20)-WC
22	Neat-23	-20	Yes	N23-(-20)-WC
23	Neat-24	-20	Yes	N24-(-20)-WC
24	Neat-25	-20	Yes	N25-(-20)-WC
25	Neat-26	Vacuum at 23	Yes	N26-V23-WC
26	Neat-27	Vacuum at 23	Yes	N27-V23-WC
27	Neat-28	Vacuum at 23	Yes	N28-V23-WC
28	Neat-29	Vacuum at 23	Yes	N29-V23-WC
29	Neat-30	Vacuum at 23	Yes	N30-V23-WC
30	Neat-31	Vacuum at 23	Yes	N31-V23-WC
31	Neat-32	Vacuum at 80	Yes	N32-V80-WC
32	Neat-33	Vacuum at 80	Yes	N33-V80-WC
33	Neat-34	Vacuum at 80	Yes	N34-V80-WC
34	Neat-35	Vacuum at 80	Yes	N35-V80-WC

Table 5.2 Summary of all 5E2N samples

Sr. No.	Sample name	Environmental conditions	Presence of crack	Abbreviation
1	5E2N-1	23	No	S1-23-NC
2	5E2N-2	23	No	S2-23-NC
3	5E2N-3	23	No	S3-23-NC
4	5E2N-4	23	Yes	S4-23-WC
5	5E2N-6	23	Yes	S6-23-WC
6	5E2N-7	23	Yes	S7-23-WC
7	5E2N-8	23	Yes	S8-23-WC
8	5E2N-9	23	Yes	S9-23-WC
9	5E2N-10	45	Yes	S10-45-WC
10	5E2N-11	45	Yes	S11-45-WC
11	5E2N-12	45	Yes	S12-45-WC
12	5E2N-13	45	Yes	S13-45-WC
13	5E2N-14	45	Yes	S14-45-WC
14	5E2N-15	60	Yes	S15-60-WC
15	5E2N-16	60	Yes	S16-60-WC
16	5E2N-17	60	Yes	S17-60-WC
17	5E2N-18	60	Yes	S18-60-WC
18	5E2N-19	60	Yes	S19-60-WC
19	5E2N-20	-20	Yes	S20-(-20)-WC
20	5E2N-21	-20	Yes	S21-(-20)-WC
21	5E2N-22	-20	Yes	S22-(-20)-WC
22	5E2N-23	-20	Yes	S23-(-20)-WC
23	5E2N-24	-20	Yes	S24-(-20)-WC
24	5E2N-25	-20	Yes	S25-(-20)-WC
25	5E2N-26	Vacuum at 23	Yes	S26-V23-WC
26	5E2N-27	Vacuum at 23	Yes	S27-V23-WC
27	5E2N-28	Vacuum at 23	Yes	S28-V23-WC
28	5E2N-29	Vacuum at 23	Yes	S29-V23-WC
29	5E2N-30	Vacuum at 23	Yes	S30-V23-WC
30	5E2N-31	Vacuum at 23	Yes	S31-V23-WC
31	5E2N-32	Vacuum at 80	Yes	S32-V80-WC
32	5E2N-33	Vacuum at 80	Yes	S33-V80-WC
33	5E2N-34	Vacuum at 80	Yes	S34-V80-WC
34	5E2N-35	Vacuum at 80	Yes	S35-V80-WC

5.3 Test Results

1. Neat and 5E2N samples without a sharp crack

Three replicates of each, neat and 5E2N samples without a sharp crack were tested on MTS machine and load vs. displacement graph was drawn as shown in Figure 5.10. In Figure 5.10, gray colored curves represent neat samples and black colored curves represent 5E2N samples. The deviation between two sets of curves clearly shows the effect of addition of microcapsules and catalyst on the critical fracture load and stiffness values of the samples. Addition of microcapsules and catalyst showed reduction in the critical fracture load and stiffness values. The nature of curves show that both types of samples fractured brittle in nature.

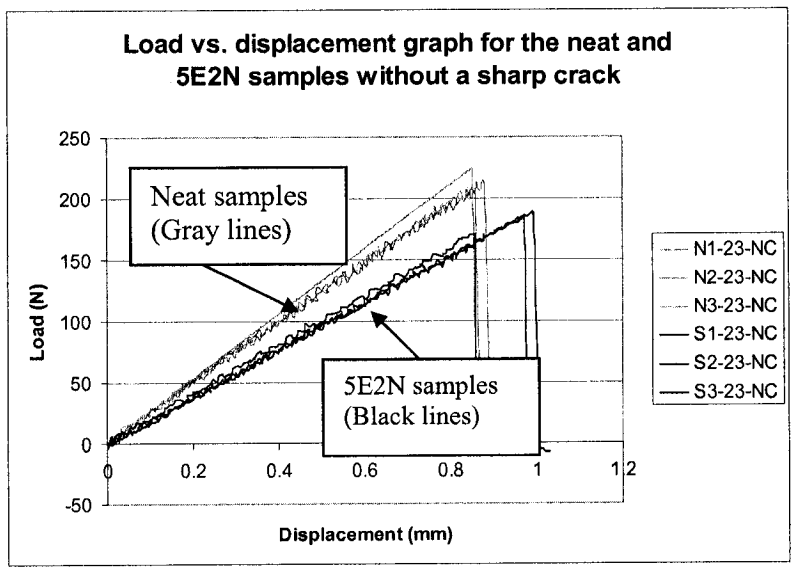

Figure 5.10 Load vs. displacement graph for neat and 5E2N samples with no sharp crack, tested at 23 °C

From Figure 5.10, the average stiffness 'S_1' of neat samples and 'S_2' of 5E2N samples were calculated and shown in Tables 5.3 and 5.4 respectively.

Table 5.3 Summary of stiffness and maximum load of neat samples without a sharp crack

Sr. No.	Sample name	Maximum Load (N)	Stiffness (N/mm)
1	N2-23-NC	208	215
2	N1-23-NC	225	265
3	N3-23-NC	214	220
Average		$P_1 = 215.6$	$S_1 = 233$

Table 5.4 Summary of stiffness and maximum load of 5E2N samples without a sharp crack

Sr. No.	Sample name	Maximum Load (N)	Stiffness (N/mm)
1	S1-23-NC	170	205
2	S2-23-NC	188	192
3	S3-23-NC	184	193
Average		$P_2 = 180.6$	$S_2 = 196$

Form table 5.3 and 5.4 it is clear that the addition of microcapsules and catalyst lowered the average maximum load of neat sample from 215.6 to 180.6 N which is about 16 %

and the average stiffness of the neat sample also reduced from 233 to 196 N/mm which is about 15.8 %.

2. Samples conditioned at 23 °C

Five replicates of neat and 5E2N samples with a sharp crack and conditioned at 23 °C were tested and load vs. displacement graph was drawn as shown in Figure 5.11. From Figure 5.11, 5E2N samples showed zigzag failure in nature. This may be due to the stick-slip phenomenon in the crack plane and crack arrest phenomenon because of presence of microcapsules and catalyst. On the contrary, most of the neat samples failed brittle in nature.

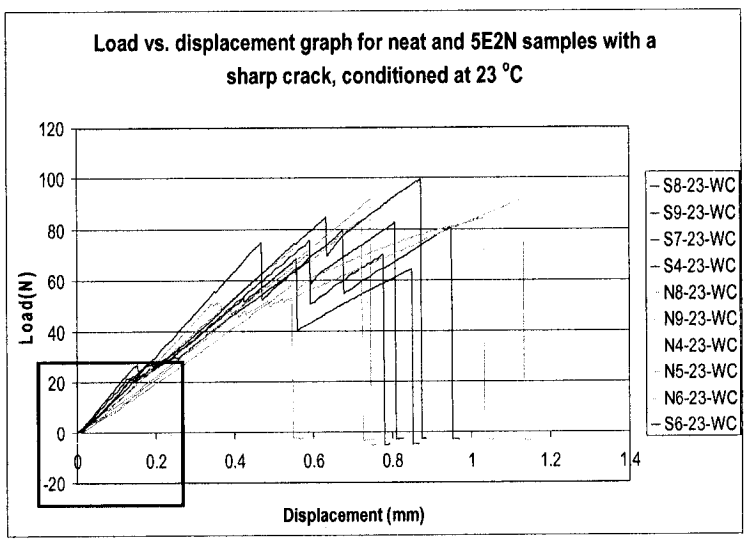

Figure 5.11 Load vs. displacement for neat and 5E2N samples with a sharp crack, conditioned at 23 °C

The enlarged view of framed portion in Figure 5.11 is shown in Figure 5.12. Figure 5.12 show that 5E2N samples are stiffer than neat samples in the presence of a sharp crack. However variation in the curves of 5E2N samples may be due to the variation in amount of healing material and the material properties of the healing material in crack plane.

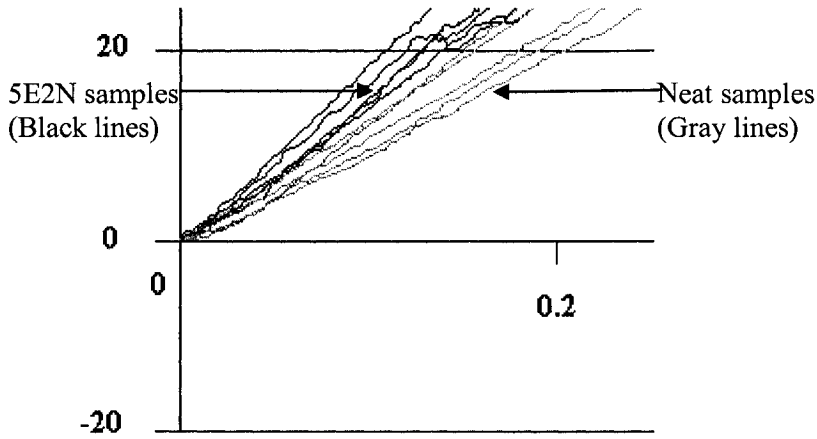

Figure 5.12 Enlarged view of framed portion shown in Figure 5.11

Table 5.5 Summary of results of 5E2N samples with a sharp crack conditioned at 23 °C

Sr. No.	Sample name	Crack length (mm)	Critical fracture load (N)	Stiffness (N/mm)	S_4/S_1 %	P_4/P_1 %	P_4/P_2 %	P_4/P_3 %
1	S4-23-WC	23	68	140	66	37	44	99
2	S6-23-WC	23	99	134				
3	S7-23-WC	32	82	180				
4	S8-23-WC	27	75	165				
5	S9-23-WC	24	80	153				
Average			$P_4 = 80.8$	$S_4 = 154.4$				

Table 5.6 Summary of results of neat samples with a sharp crack conditioned at 23 °C

Sr. No.	Sample name	Crack length (mm)	Critical fracture load (N)	Stiffness (N/mm)	S_3/S_1 %	P_3/P_1 %
1	N4-23-WC	30	84	126	49	38
2	N5-23-WC	26	91	131		
3	N6-23-WC	32	91	110		
4	N8-23-WC	28	84	105		
5	N9-23-WC	36	58	100		
Average			P_3 = 81.6	S_3=114.4		

From Tables 5.5 and 5.6 the average maximum load of neat samples is more than the average maximum load of 5E2N samples. This might be due to the crack arrest phenomenon or crack tip geometry as discussed in section 4.2. However the average stiffness of 5E2N samples is about 35 % more than the average stiffness of the neat samples. The comparison of the ratio of critical fracture loads (P_4/P_1 and P_3/P_1) does not give clear indication about healing efficiency, whereas comparison of stiffness ratios (S_4/S_1 and S_3/S_1) give clear indications of healing efficiency. The ratio P_4/P_3 shows 99 % healing efficiency.

3. Samples conditioned at 45 °C

Load vs. displacement graph for neat and 5E2N samples with a sharp crack and conditioned at 45 °C is shown in Figure 5.13. All 5E2N samples showed zigzag failure in

nature because of stick-slip and crack arrest phenomenon. Figure 5.14 shows the enlarged view of framed portion in Figure 5.13.

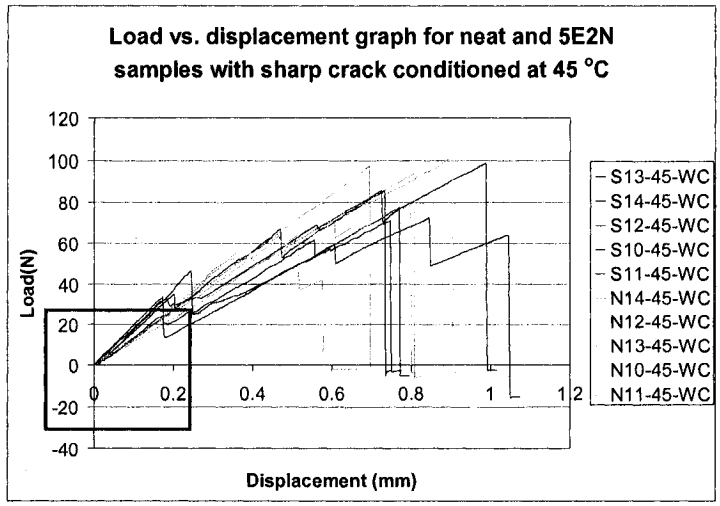

Figure 5.13 Load vs. displacement graph for the neat and 5E2N samples with sharp crack, conditioned at 45 °C

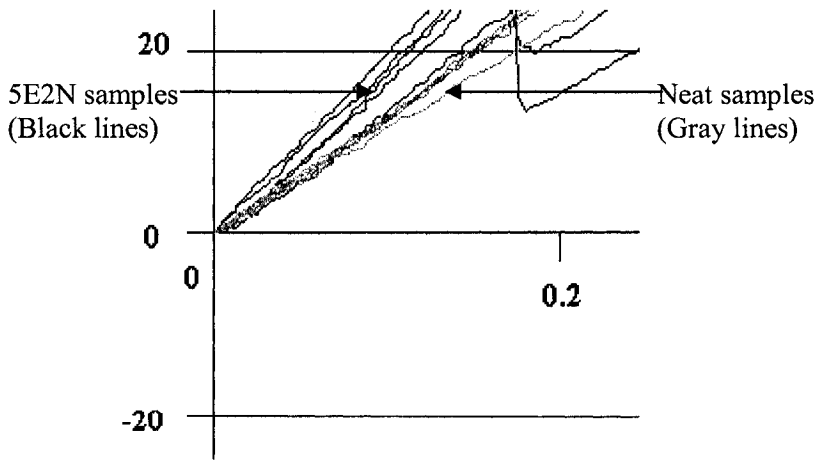

Figure 5.14 Enlarges view of framed portion shown in Figure 5.13

Table 5.7 Summary of results of 5E2N samples with a sharp crack conditioned at 45 °C

Sr. No.	Sample name	Crack length (mm)	Critical fracture load (N)	Stiffness (N/mm)	S_4/S_1 %	P_4/P_1 %	P_4/P_2 %	P_4/P_3 %
1	S10-45-WC	31	70	184	70	37	44	91
2	S11-45-WC	25	85	167				
3	S12-45-WC	27	98	179				
4	S13-45-WC	26	77	143				
5	S14-45-WC	32	65	137				
Average			$P_4 = 79$	$S_4 = 162$				

Table 5.8 Summary of the results of the neat samples with a sharp crack conditioned at 45 °C

Sr. No.	Sample name	Crack length (mm)	Critical fracture load (N)	Stiffness (N/mm)	S_3/S_1 %	P_3/P_1 %
1	N10-45-WC	24	101	136	56	40
2	N11-45-WC	24	78	130		
3	N12-45-WC	30	63	131		
4	N13-45-WC	28	97	138		
5	N14-45-WC	27	96	123		
Average			$P_3 = 87$	$S_3 = 131.6$		

The average stiffness for 5E2N samples conditioned at 45 °C is about 23 % more than the average stiffness of neat samples. The average critical fracture load of 5E2N samples as compared to P_1 (P_4/P_1) is 37 %, and the average critical fracture load of neat samples as compared to P_1 (P_3/P_1) is 40 % whereas ratio P_4/P_3 shows 91 % healing efficiency.

4. Samples conditioned at 60 °C

Figure 5.15 shows load vs. displacement graph for neat and 5E2N samples with a sharp crack and conditioned at 60 °C for healing. From Table 5.9, sample S16-60-WC with crack length of 31 mm showed the lowest critical fracture load. However the initial portion of the curve showed stiff material as result of healed crack. After breaking of the healing material the slope of the curve fall down suddenly.

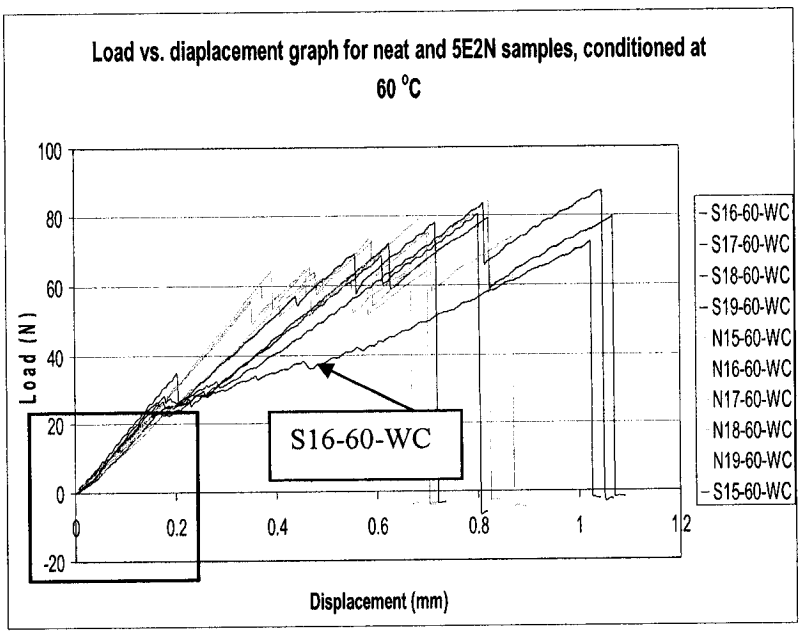

Figure 5.15 Load vs. displacement graph for neat and 5E2N samples conditioned at 60 °C

The enlarged view of framed portion in Figure 5.15 is shown in Figure 5.16.

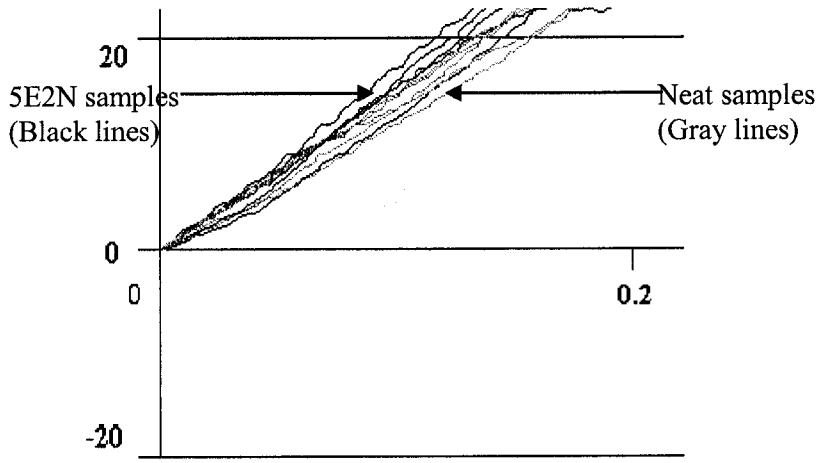

Figure 5.16 Enlarged view of framed portion in Figure 5.15

Table 5.9 Summary of results of 5E2N samples with a sharp crack conditioned at 60 °C

Sr. No.	Sample name	Crack length (mm)	Critical fracture load (N)	Stiffness (N/mm)	S_4/S_1 %	P_4/P_1 %	P_4/P_2 %	P_4/P_3 %
1	S15-60-WC	25	77	160	66	37	44	107
2	S16-60-WC	31	72	157				
3	S17-60-WC	24	86	149				
4	S18-60-WC	26	80	169				
5	S19-60-WC	26	79	135				
Average			P_4 = 78.8	S_4 =154				

Table 5.10 Summary of the results of the neat samples with a sharp crack conditioned at 60 °C

Sr. No.	Sample name	Crack length (mm)	Critical fracture load (N)	Stiffness (N/mm)	S_3/S_1 %	P_3/P_1 %
1	N15-60-WC	22	66	144	59	34
2	N16-60-WC	26	84	127		
3	N17-60-WC	24	64	149		
4	N18-60-WC	23	80	146		
5	N19-60-WC	25	73	123		
Average			P_3 = 73.4	S_3 =137.8		

In contrast to the previous two tests, the average maximum load of 5E2N sample in this case, P_4 = 78.8 N and that of neat sample, P_3 = 73.4 N. The average stiffness for 5E2N samples is about 11.7 % more than the average stiffness of the neat samples. In this case, ratio P_4/P_3 shows 107 % healing of samples.

5. Samples conditioned at 100 °C

5E2N samples conditioned at 100 °C were obtained in distorted shape. Figure 5.17 shows schematic drawing of sample in good condition and sample in distorted shape.

(a) (b)

Figure 5.17 (a) Schematic representation of sample in good condition and (b) distorted sample due to conditioning at 100 °C

The reason for this phenomenon might be the presence of liquid phase in form of microcapsules in the material. But more tests need to be done to validate this reason.

For practical applications, change in the shape of the structure is not desirable as it induces internal stresses and loses the integrity with other structure. As such no more further testing for the samples conditioned at 100 °C was done.

6. Samples conditioned at -20 °C

Six replicates of neat and 5E2N samples with a sharp crack and conditioned at -20 °C were tested and load vs. displacement graph was drawn as shown in Figure 5.18. Few neat samples show zigzag failure in nature. This may be due to only crack arrest phenomenon as there is no healing material in the crack plane. As shown in Figure 5.18, sample 'S25-(-20)-WC' with crack length of 52 mm showed critical fracture load of 50 N. However due to healed crack, the initial portion of load-displacement plot showed stiff material.

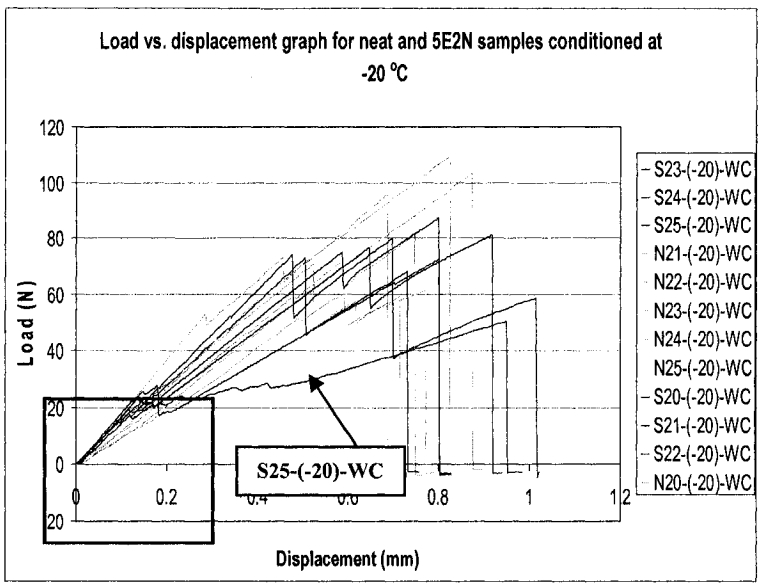

Figure 5.18 Load vs. displacement graph for neat and 5E2N samples conditioned at -20 °C

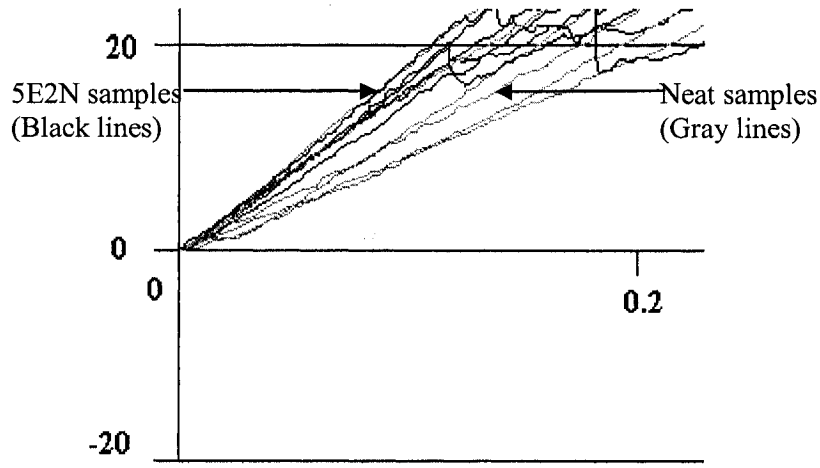

Figure 5.19 Enlarged view of framed portion in Figure 5.18

Similar to all the previous cases the enlarged view of framed portion in Figure 5.18 as shown in Figure 5.19 shows stiffening effect in 5E2N samples because of healed crack. As such at -20 °C 5E2N samples showed healing of crack.

Table 5.11 Summary of results of 5E2N samples with a sharp crack conditioned at -20 °C

Sr. No.	Sample name	Crack length (mm)	Critical fracture load (N)	Stiffness (N/mm)	S_4 / S_1 %	P_4 / P_1 %	P_4 / P_2 %	P_4 / P_3 %
1	S20-(-20)-WC	29	81	165	70	34	41	85
2	S21-(-20)-WC	37	72	162				
3	S22-(-20)-WC	26	87	177				
4	S23-(-20)-WC	24	72	162				
5	S24-(-20)-WC	22	79	145				
6	S25-(-20)-WC	52	50	162				
Average			$P_4 = 73.5$	$S_4 = 162$				

Table 5.12 Summary of results of neat samples with sharp crack conditioned at -20 °C

Sr. No.	Sample name	Crack length (mm)	Critical fracture load (N)	Stiffness (N/mm)	S_3/S_1 %	P_3/P_1 %
1	N20-(-20)-WC	29	70	135	53	40
2	N21-(-20)-WC	24	81	115		
3	N22-(-20)-WC	25	95	115		
4	N23-(-20)-WC	33	61	95		
5	N24-(-20)-WC	22	109	184		
6	N25-(-20)-WC	29	103	98		
Average			P_3= 86.5	S_3= 123.6		

From Tables 5.11 and 5.12 the average stiffness of 5E2N samples as compared to S_1 (ratio S_4/S_1) is 32 % more than the average stiffness of neat samples (ratio S_3/S_1). The average critical fracture load of 5E2N samples as compared to P_1 is (P_4/P_1= 34 %) less than that of neat samples (P_3/P_1 = 40 %). The ratio P_4/P_3 shows 85 % healing of samples conditioned at -20 **°C.**

7. Samples conditioned at 23 °C in vacuum at $10^{-6} mbar$ **:**

Load vs. displacement graph for neat and 5E2N samples with a sharp crack conditioned at 23 °C under vacuum ($10^{-6} mbar$) is shown in Figure 5.20. Similar to the previous test results, the curves shown in Figure 5.20 represent zigzag failure in nature of neat and 5E2N samples. As mentioned before this may be due to crack arrest phenomenon and stick-slip phenomenon in 5E2N samples.

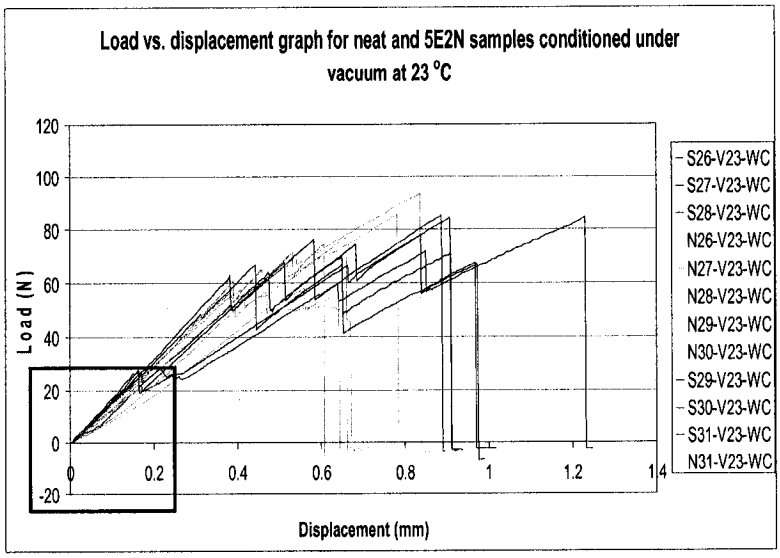

Figure 5.20 Load vs. displacement graph for neat and 5E2N samples with a sharp crack conditioned at 23 °C under vacuum (10^{-6} *mbar*)

The enlarged view of curves is shown in Figure 5.21, 5E2N samples showed higher slope than neat samples. As such 5E2N samples showed healing of crack even in vacuum.

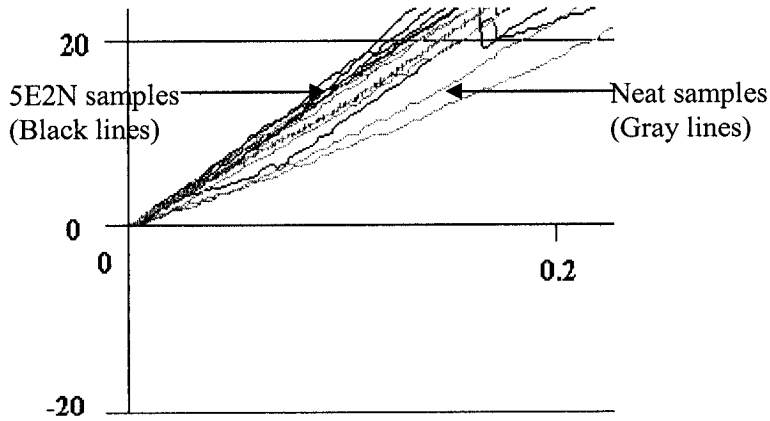

Figure 5.21 Enlarged view of framed portion in Figure 5.20

Table 5.13 Summary of results of 5E2N samples with a sharp crack, conditioned at 23 °C under vacuum (10^{-6} *mbar*)

Sr. No.	Sample name	Crack length (mm)	Critical fracture load (N)	Stiffness (N/mm)	S_4/S_1 %	P_4/P_1 %	P_4/P_2 %	P_4/P_3 %
1	S26-V23-WC	32	84	127	66	36	43	107
2	S27-V23-WC	31	85	151				
3	S28-V23-WC	26	66	151				
4	S29-V23-WC	33	77	158				
5	S30-V23-WC	24	84	162				
6	S31-V23-WC	22	71	171				
Average			P_4 = 77.8	S_4 = 153.3				

Table 5.14 Summary of results for neat samples with a sharp crack, conditioned at 23 °C under vacuum (10^{-6} *mbar*)

Sr. No.	Sample name	Crack length (mm)	Critical fracture load (N)	Stiffness (N/mm)	S_3/S_1 %	P_3/P_1 %
1	N26-V23-WC	26	58	147	54	34
2	N27-V23-WC	24	85	145		
3	N28-V23-WC	26	77	109		
4	N29-V23-WC	27	93	126		
5	N30-V23-WC	32	51	92		
6	N31-V23-WC	23	74	138		
Average			P_3 = 73	S_3 = 126.1		

The average stiffness of six 5E2N samples is 153.3 and that of neat samples is 126.1 N/mm. Healed crack increased the average stiffness of 5E2N samples by 22 % than neat samples. The average critical fracture load of the 5E2N samples is 77.8 and of neat samples is 73 N. As such critical fracture load of a sample may not be indicative of healing efficiency. The ratio P_4 / P_3 shows samples conditioned at 23 °C under vacuum healed 107 %.

8. Samples conditioned at 80 °C under vacuum (10^{-6} *mbar*)

The samples were taken out of the vacuum chamber and their temperatures were measured. Though the temperature of heating foil was set at 80 °C, the temperatures of the samples were found out around 100 °C. The 5E2N samples were found to be in soft phase. Also it was observed that the heating arrangement used for this test did not show uniform heating of the samples. As such results are not included here.

In comparison with the results obtained from the group at Illinois University (Figure 4.2) where a healing efficiency of 90 % was achieved at room conditions, the results obtained from this work shows the following healing efficiency (using the same basis of comparison at the group at Illinois):

- At 23 °C, 99 %
- At 45 °C, 90 %
- At 60 °C, 107 %
- At -20 °C, 85 %
- At 23 °C in vacuum (10^{-6} *mbar*), 107 %

9. Thermal shock test:

Figure 5.22 shows the neat sample and 5E2N sample subjected to thermal shock test and Figure 5.23 shows healed cracks in 5E2N sample.

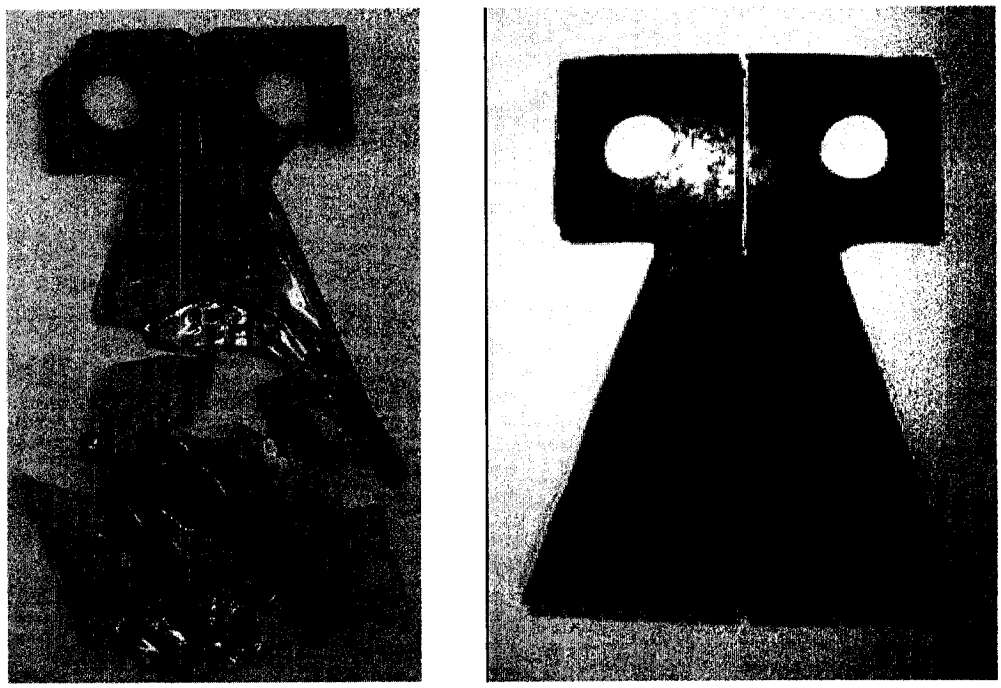

(a) (b)

Figure 5.22 Thermal shock test: (a) Neat sample, (b) 5E2N sample [36]

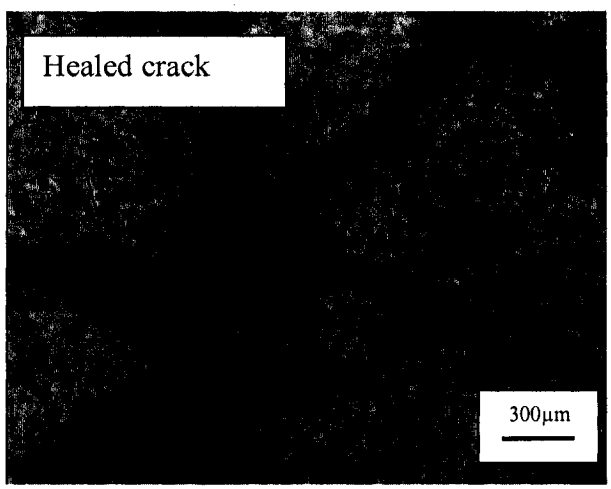

Figure 5.23 5E2N samples with crack healed with healing material [36]

From Figure 5.22 it is clear that many cracks were formed within the neat and 5E2N samples subjected to the thermal cycle. After 20 thermal cycles, the neat sample was broken into pieces while inspite of having many cracks in the 5E2N sample; the sample remained in one piece.

Figure 5.23 shows that the empty microcapsules in the crack path which show that the cracks formed due to thermal shock were healed with the healing material.

10. Young's modulus 'E_2' of healing material:

Table 5.15 Young's modulus of polymerized 5E2N monomer with 1 % of Grubbs' catalyst

Sr. No.	Sample name	Young's Modulus 'E_2' (GPa)
1	Sample-1	0.102
2	Sample-2	0.086
3	Sample-3	0.053
4	Sample-4	0.087

Summary of Young's modulus (E_2) of polymerized 5E2N monomer with 1 % of Grubbs' catalyst are shown in Table 5.15. These values are only for 1 % catalyst and give an overall idea about E_2. In practice this percentage of Grubbs' catalyst in relation to the monomer quantity may vary at crack sites due to random distribution of microcapsules and catalyst. As such for ANSYS®10.0 analysis in chapter 6, different values of E_2 = 1, 0.1 and 0.01 GPa were used.

5.4 Microscopic observations of fractured crack surface

The crack in the sample and fractured crack surfaces of 5E2N and neat samples were observed under the microscope.

The 5E2N samples with crack were observed under the microscope. The crack propagation phenomenon broke the microcapsules in the path and healing material inside the microcapsule flowed into the crack as shown in Figure 5.24.

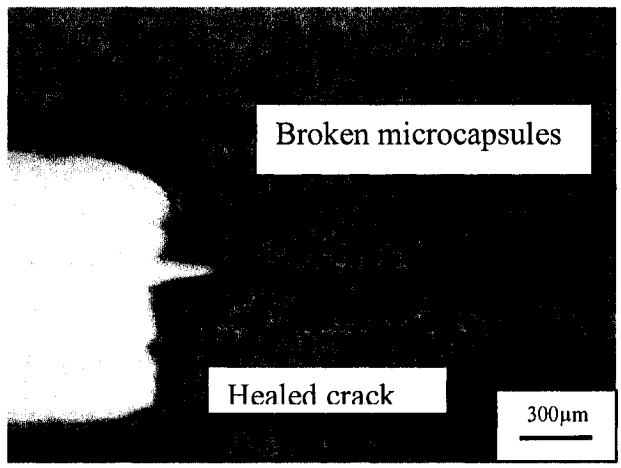

Figure 5.24 5E2N sample with healed crack

The fractured crack surface of the 5E2N sample was studied. The polymerized film of healing material was observed over the crack surface. The dividing line as shown in Figure 5.25 clearly shows healed crack with thin film of healing material and unhealed portion (portion ahead of the crack tip).

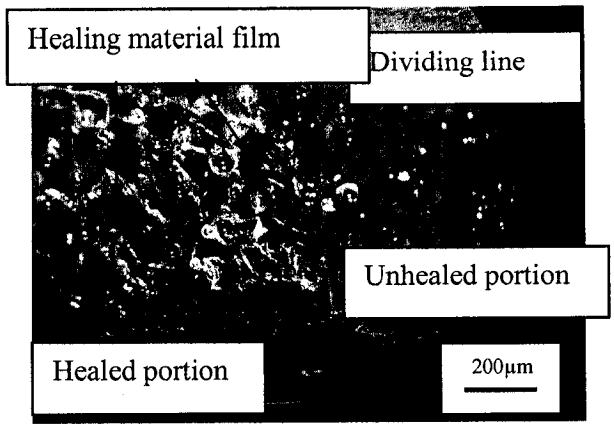

Figure 5.25 5E2N sample with dividing line showing healed portion and unhealed portion

The observation of fractured crack surfaces of 5E2N and neat sample showed that there is no healing process in the neat sample which was expected. As shown in Figure 5.26, the 5E2N sample has rough crack surface with thin film of healing material, but the crack surface of the neat sample is shiny and smooth.

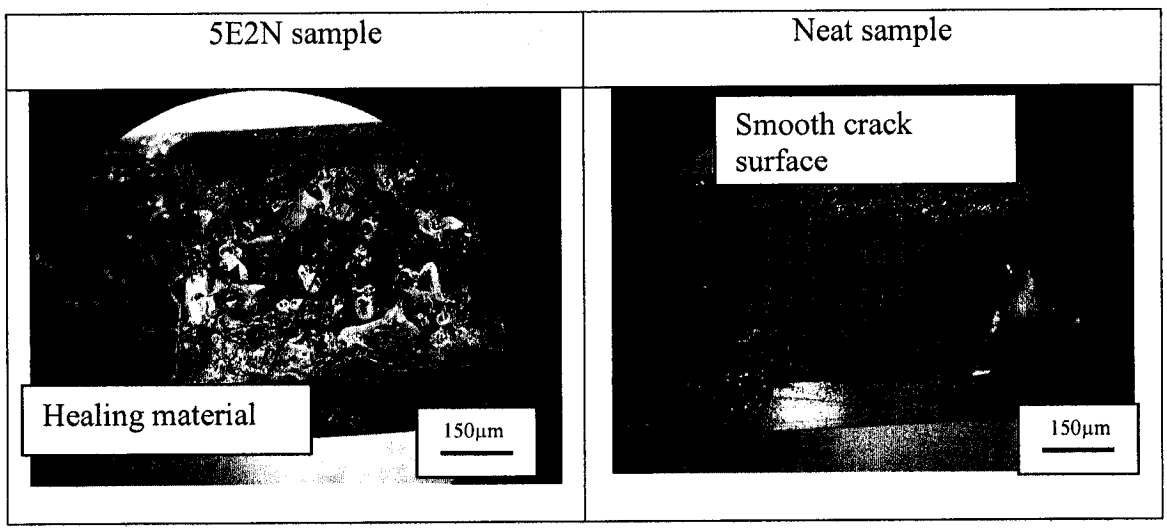

Figure 5.26 Crack surfaces of 5E2N and neat sample

Chapter 6

Finite Element Analysis using ANSYS® 10.0

6.1 ANSYS Utilization

Finite element analysis was done using ANSYS® 10.0 and experimental results were compared with ANSYS results. ANSYS® is analysis software for finite element analysis and design [37].

Tapered Double Cantilever Beam specimen (TDCB) was modeled in CATIA V5R15 and imported into ANSYS® 10.0 for finite element analysis as shown in Figure 6.1.

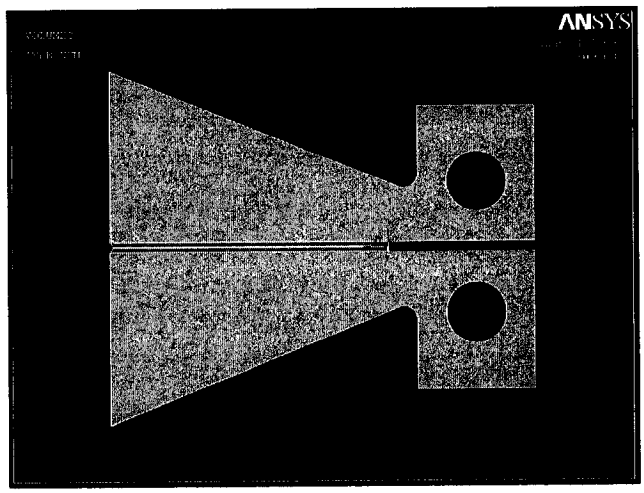

Figure 6.1 TDCB model in ANSYS® 10.0

Due to irregularity of TDCB specimen, SOLID-92 3-D 10 node Tetrahedral Structural Solid element (Figure 6.2) was selected for meshing TDCB shape.

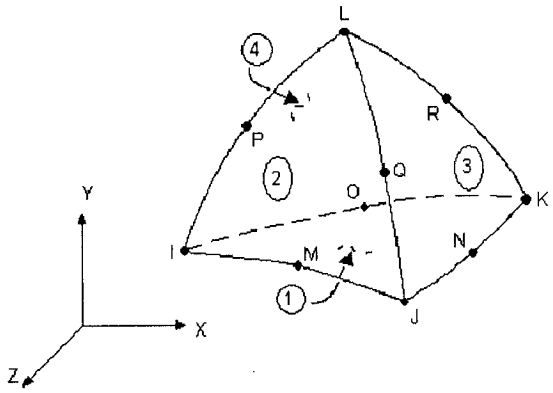

Figure 6.2 SOLID92 3-D 10-Node Tetrahedral Structural solid element [38]

Healing material in the crack plane was represented by a separate volume covering a certain amount of crack. This volume was meshed using SOLID186 elements and was assigned different material properties. This volume was bonded to the two crack faces to act as bonding material as shown in Figure 6.3.

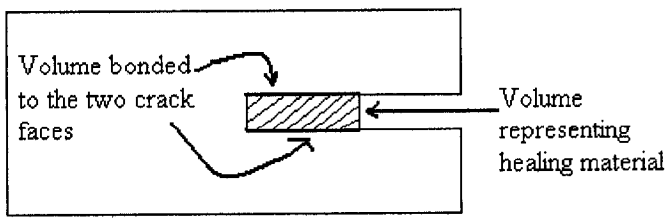

Figure 6.3 Volume representing healing material and bonded to the crack faces

SOLID186 3-D 20 node element was used for the healing material (Figure 6.4). This element has three degrees of freedom per node: translations in the nodal x, y, and z directions [39].

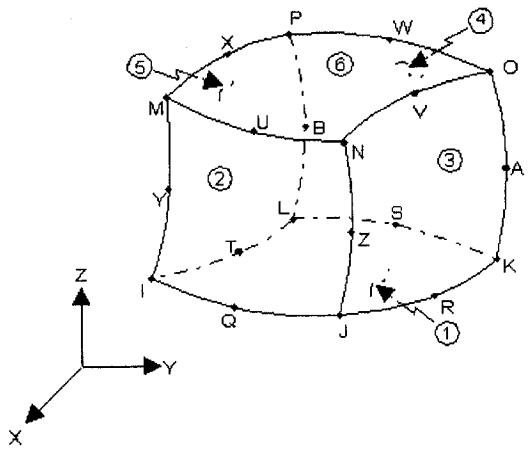

Figure 6.4 SOLID186 3-D 20-Node structural solid element [39]

The TDCB model was meshed using above two types of element as shown in Figure 6.5.

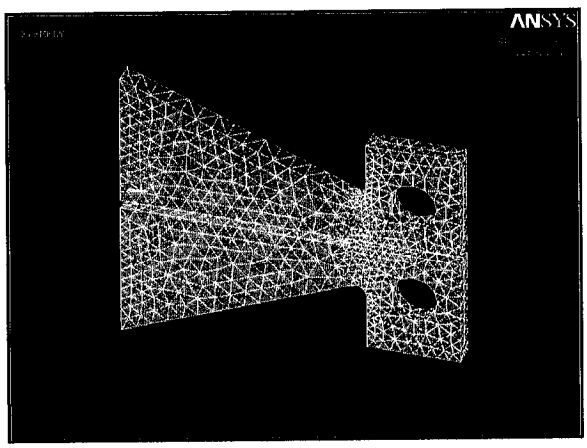

Figure 6.5 Meshed TDCB model

6.2 Assumptions made for ANSYS® analysis

For the ANSYS® analysis a few assumptions were made for simplification. These assumptions regarding crack representation and healing of crack are discussed as follows.

In actual case the samples may have crack with sharp tip. In ANSYS®, a crack was represented by a small gap of 0.1 mm between two faces as shown in Figure 6.6. As such a crack tip does not have sharp tip end.

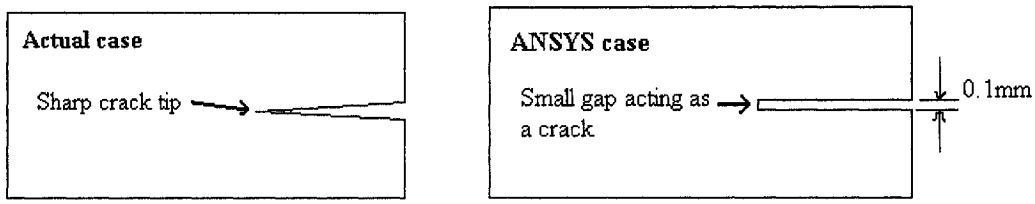

(a) (b)

Figure 6.6 (a) Actual case showing sharp crack tip, (b) ANSYS® model, gap representing crack

Healing analysis was done for different percentages of healed crack. Assume that there is 25 % healing of crack. In real case the healing material heals 25 % of the crack randomly. Due to random distribution of microcapsules in the material, at some portion of a crack there will be healing material and at some other portion there will not be.

In ANSYS® it was assumed that 25 % of the crack was healed uniformly from the crack tip. Both the cases are schematically represented as shown in Figure 6.7.

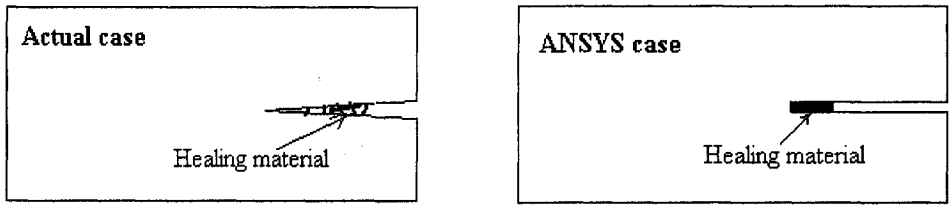

Figure 6.7 Schematic representation of healed crack in real case and in ANSYS®

From experimental results it was observed that the maximum fracture loads for all samples varied in the range 50 N to 130 N. For analysis purpose 100 N was selected as maximum fracture load and the displacement of a specific node was recorded.

In ANSYS®, 100 % healed crack was represented as a crack healed uniformly with healing material as shown in Figure 6.8b. In real case, the samples having the healing material in their crack plane almost at the crack beginning edge was considered as 100 % healed sample (Figure 6.8a).

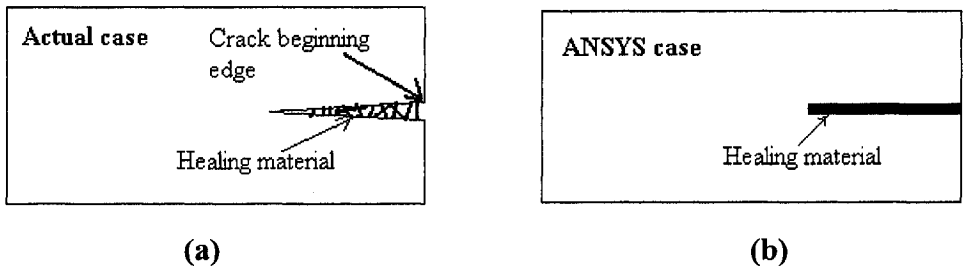

Figure 6.8 Samples with 100 % healed crack (a) real case, (b) ANSYS® model

6.3 Determination of Stiffness

The stiffness values were determined from ANSYS® analysis and these stiffness values were compared with experimental results. The encircled portion in figure 6.9 shows the crack location and the enlarged view of this portion was used in the following discussion.

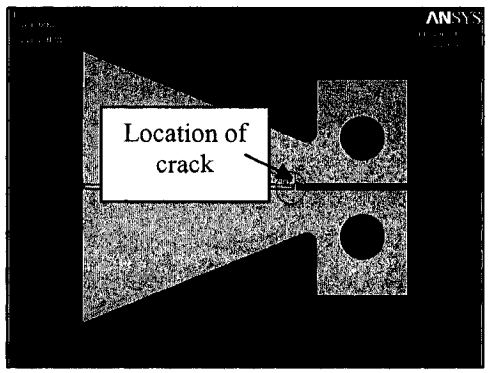

Figure 6.9 Encircled portion representing a crack location

The general procedure followed for ANSYS analysis is discussed below.

1. A crack of desired length was created in the TDCB model. Figure 6.10 shows TDCB model with crack length a = 22 mm.

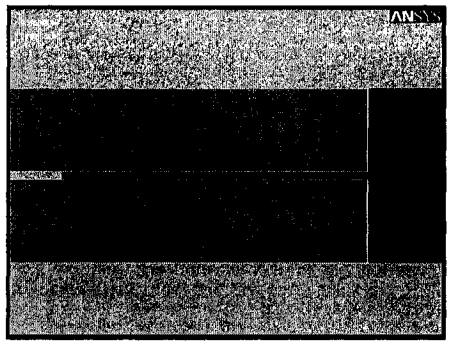

Figure 6.10 TDCB model with crack length a = 22 mm

2. A portion of the crack was filled with a separate volume to represent the healed crack. Then this volume was bonded to the crack faces. Figure 6.11 represents sample with crack length 22 mm and healed 50 %.

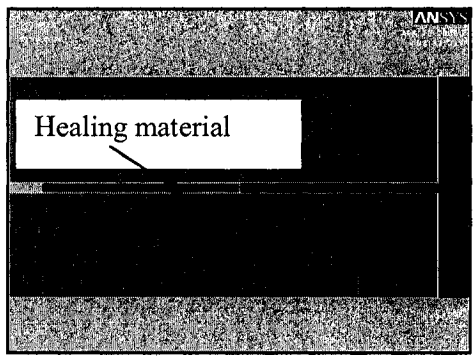

Figure 6.11 Sample with crack length a = 22 mm and 50 % healed crack

3. As shown in Figure 6.12, TDCB portion indicated by number '1' was meshed with SOLID92 elements. The material properties such as Young's modulus 'E_1' and Poisson's ratio 'ν_1' were assigned to it and the portion indicated by number

'2' is healing material and meshed with SOLID186 element and material properties such as Young's modulus 'E_2' and Poisson's ratio 'ν_2' were assigned to it.

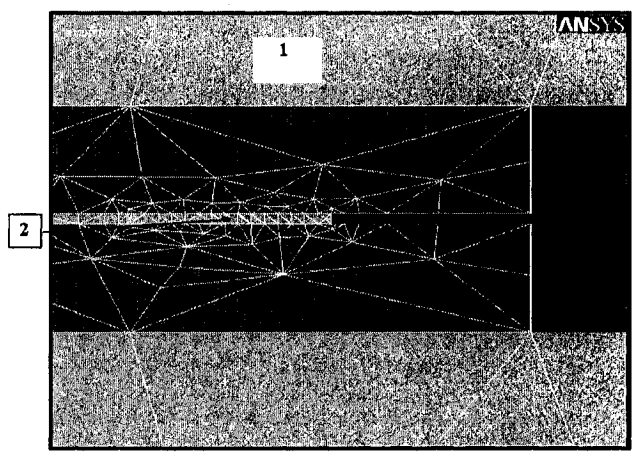

Figure 6.12 Sample showing different numbering system for TDCB sample material and healing material

4. Load was applied in a similar fashion like on MTS machine. An upper arm of the TDCB specimen was fully constrained and tensile load was applied at the three nodes on the lower arm as shown in Figure 6.13.

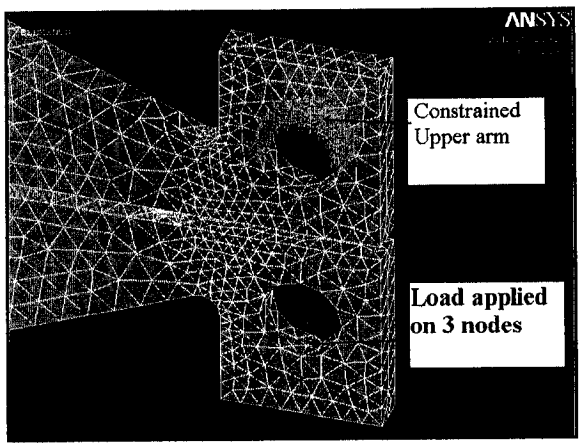

Figure 6.13 Constrained and loaded TDCB model

5. Tensile load of 100 N was applied perpendicular to the crack plane and the displacement at the node location as shown in Figure 6.14 in the 'y' direction perpendicular to the crack plane was considered. This node displacement mimics the lower head displacement of MTS machine.

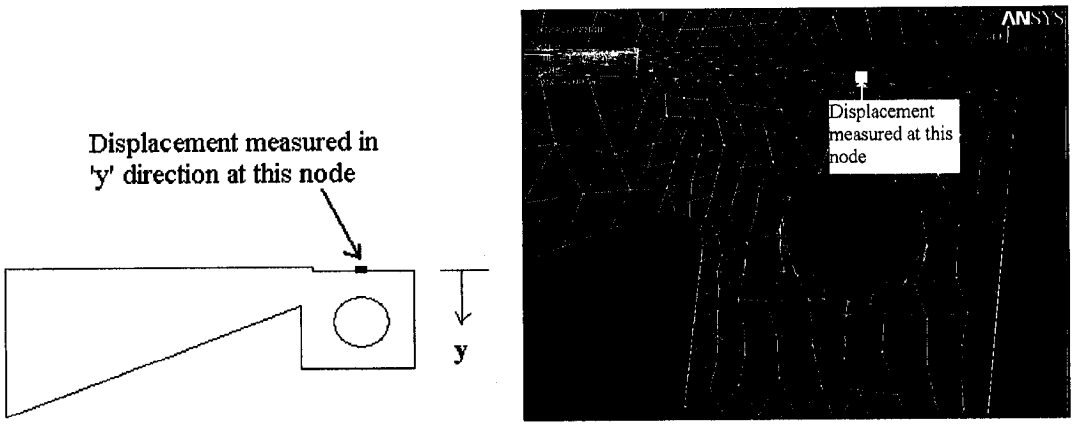

Figure 6.14 Sample showing the location where of node displacement perpendicular to the crack plane were measured (in y direction)

6.4 Different test parameters for ANSYS® analysis

ANSYS® analysis was carried out for different parameters such as crack length, material properties, % of healed crack and material properties of healed material. This is explained in more details as follows.

- ANSYS® analysis was done for different crack lengths from 20 to 28 mm.

- In reality, % healed portion of a crack varies from sample to sample because the amount of microcapsules present at crack site varies from sample to sample. This fact was considered and ANSYS® analysis was done for different % of healed crack. ANSYS® analysis was done for 0 %, 25 %, 50 %, 75 % and 100 % healed portion of crack plane. The 0 % healed samples have no healing material in the crack plane and considered as the neat samples.

- Material properties of healed material depend upon the amount of the catalyst present at crack site. Though in reality 1 % of the catalyst was added to the sample, at crack site this percentage may vary. Considering this, analysis was done for different properties of the healed material E_2.

6.5 ANSYS® Results

A] Effect of E_2 on the stiffness values:

The material properties E_1 = 3.5 GPa [30] was chosen. Three values of E_2 = 1, 0.1, and 0.01 GPa were selected from experimental results as discussed in section 5.2. The majority of engineering materials have Poisson's ratio from 0.2 to 0.4. For analysis purpose ν_1 = 0.2 and ν_2 = 0.3 were chosen. Table 6.1 shows the stiffness of samples for different values of E_2.

Table 6.1 Stiffness of samples for different E_2 values and different % of healed crack (E_1 = 3.5 GPa, ν_1 = 0.2, ν_2 = 0.3)

		Stiffness values for different % healed crack (N/mm)				
Crack Length 'a' (mm)	Young's modulus 'E_2' (Pa)	0 %	25 %	50 %	75 %	100 %
20	1.00E+09	150.4	153.4	157	160	161.5
	1.00E+08	150.4	151.4	153.4	155.6	157.4
	1.00E+07	150.4	150.5	150.9	151.4	152
22	1.00E+09	136.7	142.3	149.3	156.6	161.4
	1.00E+08	136.7	139.1	143.7	149.4	154.5
	1.00E+07	136.7	137.11	138.1	139.7	141.8
24	1.00E+09	125.2	132.4	141.9	152.8	161.3
	1.00E+08	125.2	128.7	135.4	144.3	153
	1.00E+07	125.2	125.9	127.5	130.5	134.5
26	1.00E+09	115.5	123.9	135.5	148.9	161.2
	1.00E+08	115.5	120.1	128.5	139.9	152.3
	1.00E+07	115.5	116.5	118.9	123.3	129.5
28	1.00E+09	107.9	116.7	129.2	145	161.2
	1.00E+08	107.9	112.9	122.6	136.5	151.8
	1.00E+07	107.9	108.9	112.1	117.8	126.27
Average (N/mm) (For E_2 = 0.1 GPa)		127.1	130.4	136.7	145.1	153.8

From Table 6.1, stiffness vs. % healed crack graphs were made for three different values of E_2 as shown in Figures 6.15, 6.16 and 6.17. In all the graphs the legend box consist of different crack length from a = 20 to 28 mm used for ANSYS analysis and 5E2N(exp) represents average stiffness values of 5E2N samples from all experimental results. The average experimental stiffness value of 5E2N samples is 157.1 N/mm.

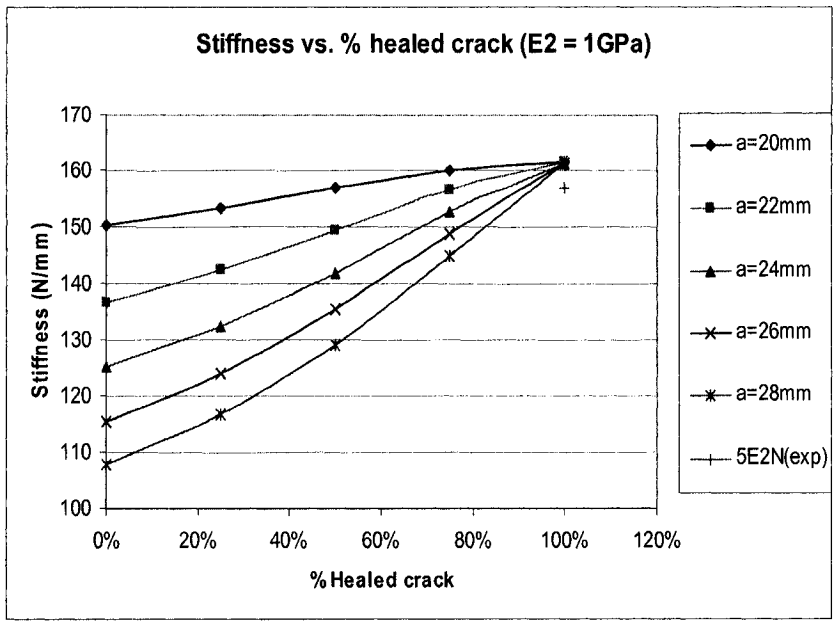

Figure 6.15 Stiffness vs. % healed crack graph for E_2 = 1 GPa, E_1 = 3.5 GPa, ν_1 = 0.2 and ν_2 = 0.3

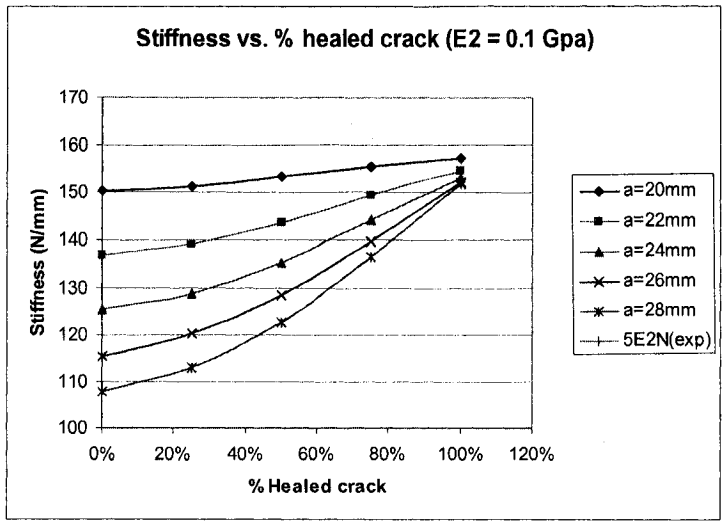

Figure 6.16 Stiffness vs. % healed crack graph for $E_2 = 0.1$ GPa, $E_1 = 3.5$ GPa, $\nu_1 = 0.2$ and $\nu_2 = 0.3$

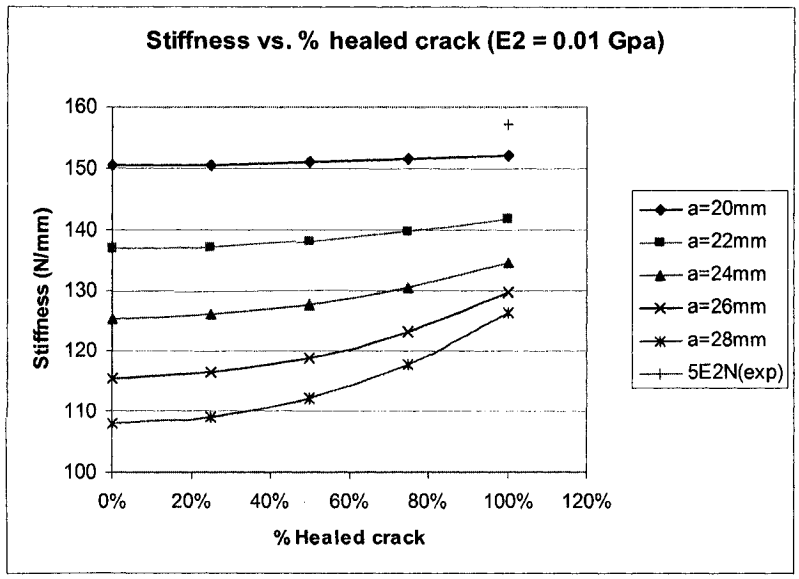

Figure 6.17 Stiffness vs. % healed crack graph for $E_2 = 0.01$ GPa, $E_1 = 3.5$ GPa, $\nu_1 = 0.2$ and $\nu_2 = 0.3$

The stiffness vs. crack length graph for different healing material properties E_2 is shown in Figure 6.18.

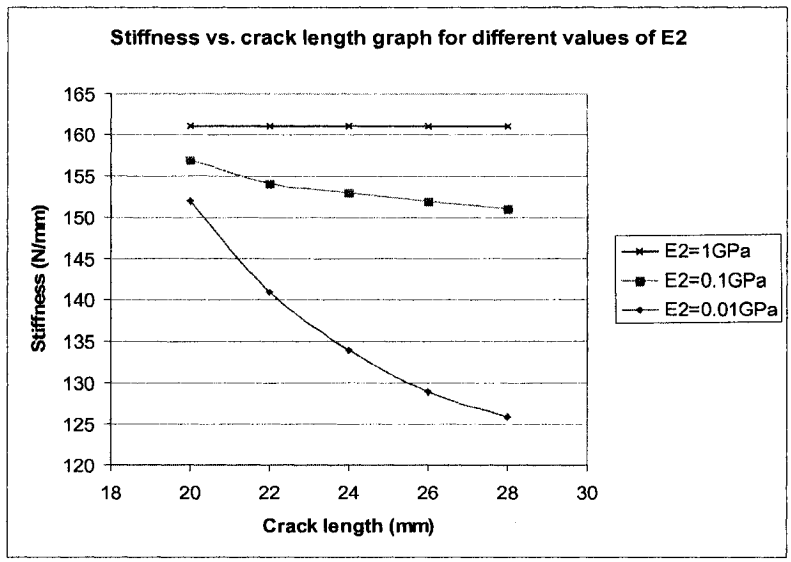

Figure 6.18 Stiffness vs. crack length graph for different values of E_2 (E_1= 3.5 GPa, ν_1 = 0.2 and ν_2 = 0.3)

From the above graphs the following observations can be made.

1. Figures 6.15 and 6.16 show that due to healed crack, the stiffness values for 100 % healed samples with different crack length are almost same.

2. Figure 6.17 show that for the value of E_2 = 0.01 GPa, 100 % healed samples did not show significant improvement in the stiffness value. These stiffness values are

almost same as that of 0 % healed samples. This may be because healing material is not stiff enough to keep the crack faces together.

3. Figure 6.18 show that as far as healing material is strong enough, crack length did not show any effect in the stiffness values.

B] Effect of E_1 on the stiffness values:

Addition of microcapsules and catalyst may change the Young's modulus of the material. The analysis was carried out for different values of E_1. The Young's modulus E_1 of the neat epoxy is 3.5 GPa [30]. Different values of E_1 = 3.3 and 3.1 GPa were chosen for analysis purpose [30]. Young's modulus E_2 = 0.1 GPa and Poisson's ratio ν_1 = 0.2 and ν_2 = 0.3 were selected. The analytical results are summarized in Table 6.2.

Table 6.2 Stiffness of samples for different E_1 values and different % of healed crack (E_2 = 0.1 GPa, ν_1 = 0.2, ν_2 = 0.3)

		Stiffness values for different % healed crack (N/mm)				
Crack Length 'a' (mm)	Young's modulus 'E_1' (Pa)	0 %	25 %	50 %	75 %	100 %
20	3.3E+09	141.89	142.81	144.77	146.91	148.62
	3.1E+09	133.29	134.2	136.09	138.14	139.76
22	3.3E+09	128	131	135	141	146
	3.1E+09	121.16	123	127.66	132	137
24	3.3E+09	118.11	121.54	127.96	136.4	144.68
	3.1E+09	110.95	114.27	120.42	128.46	136.26
26	3.3E+09	108.95	113.36	121.46	132.35	144
	3.1E+09	102.34	106.61	114.33	124.68	135.66
28	3.3E+09	101.75	106.61	115.87	128.77	143.64
	3.1E+09	95.58	100.27	109.09	121.32	135.34
Average (N/mm) (For E_1 = 3.3 GPa)		119.74	123.06	129.01	137.08	145.38

From Table 6.2 the load vs. displacement graphs were plotted as shown in Figure 6.19 and 6.20.

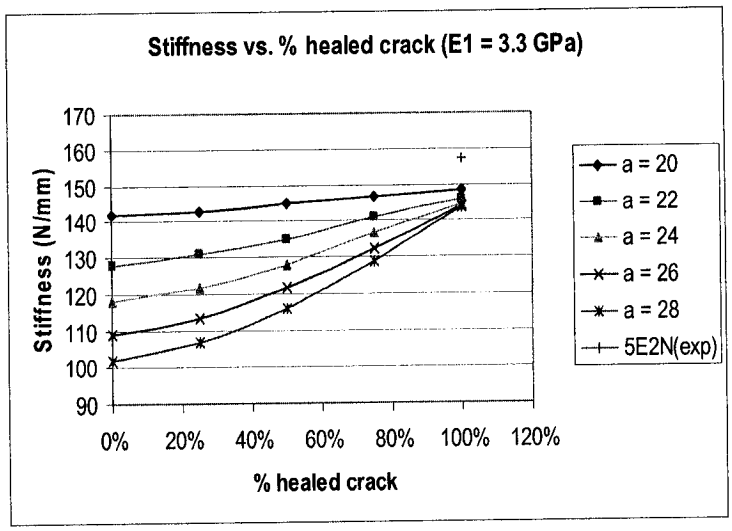

Figure 6.19 Stiffness vs. % healed crack plot for E_1= 3.3 GPa, E_2 = 0.1 GPa, ν_1 = 0.2 and ν_2 = 0.3

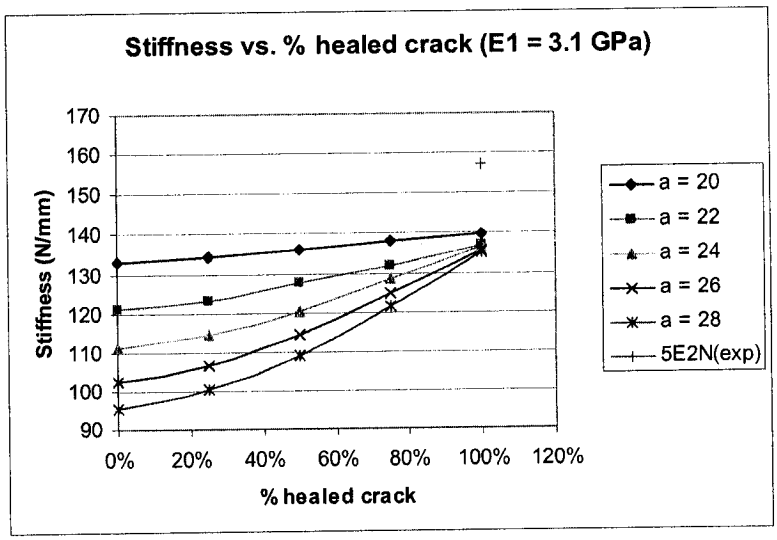

Figure 6.20 Stiffness vs. % healed crack plot for E_1= 3.1 GPa, E_2 = 0.1 GPa, ν_1 = 0.2 and ν_2 = 0.3

From Figures 6.19 and 6.20 the following observations can be made.

1. For E_1 = 3.3 GPa, the average stiffness value of the 100 % healed samples was obtained as 145.3 N/mm. The experimental average stiffness value of 5E2N samples is 157.1 N/mm. The difference between ANSYS and experimental results may be due to the property of the healed material. Though E_2 = 0.1 GPa was used in ANSYS analysis, in reality this value may be different.

2. As the value of E_1 changed from 3.3 to 3.1 GPa, stiffness of 100 % healed sample is reduced from 145.3 N/mm to 136.8 N/mm.

Chapter 7

Discussion

The new monomer 5-ethyledene-2-norbornene with a wide liquid temperature range (-80 °C to +146 °C) was examined as a healing material. Between the 5E2N and DCPD monomer, it was observed that the 5E2N provides a better option as a healing agent for space application than the DCPD.

The new approach was used to determine the healing efficiency. The initial portion of load vs. displacement graph was used to calculate stiffness values of the samples to determine the healing efficiency. The average stiffness comparison between neat samples (unhealed samples) and 5E2N samples (healed samples) gave clear idea about healing of a crack plane.

The determination of healing efficiency is explained. Consider the case of the samples conditioned at 23 °C. The average stiffness of the neat and 5E2N samples without a sharp crack are S_1 = 233 N/mm and S_2 = 196 N/mm respectively. The average stiffness of the neat and 5E2N samples with a sharp crack and healed for one day at 23 °C are S_3 = 114.4 N/mm and S_4 = 154.4 N/mm respectively. In the presence of sharp crack, the % stiffness of the neat sample in comparison with S_1 is 49 % (S_3/S_1 = 114.4/233). Similarly the % stiffness of 5E2N samples with sharp crack and healed for one day, in comparison with S_1 is 66.26 % (S_4/S_1 = 154.4/233). These two values clearly show that

the healing process in a crack plane recovered the stiffness value in case of 5E2N samples. The summary of the % stiffness recovered for all tests is given in Table 7.1.

Table 7.1 Summary of % recovery of stiffness value of 5E2N and neat samples

		% stiffness recovered	
Sr. No.	Different Tests	5E2N sample (S_4/S_1)	Neat sample (S_3/S_1)
1	23 °C	66.26	49.09
2	45 °C	69.52	56.48
3	60 °C	66.09	59.14
4	-20 °C	69.52	53.04
5	Vacuum at 23°C	65.79	54.12

Table 7.1 shows the summary of results of the samples healed at 23, 45, 60,-20 °C and in vacuum at 23 °C. In all of these tests the % stiffness recovered of 5E2N samples (S_4/S_1) is more than the % stiffness recovered of neat samples (S_3/S_1). In case of the 5E2N samples there is healing material in the crack plane which binds the two crack faces together. But as expected the neat samples did not show this phenomenon. As such healed 5E2N samples showed improvement in the recovery of the stiffness values as compared to the neat samples.

The 5E2N samples tested in vacuum, showed improvement in the recovery of stiffness values (S_4/S_1 = 65.79 N/mm) as compared with the neat samples (S_3/S_1 = 54.12 N/mm). As such for this test vacuum did not show any detrimental effect on the healing process. The polymerization reaction time between 5E2N and Grubbs' catalyst was fast enough to polymerize 5E2N before it flows out of the crack.

The 5E2N samples subjected to the thermal cycles remained united due to healing, instead of falling into pieces just like neat samples. The formation of crack due to thermal shock broke the microcapsules in their path, allowing healing material to flow into the crack and polymerized with catalyst.

The microscopic observations of fractured surface of the crack plane revealed that the 5E2N monomer free-flowed into the crack plane forming polymerized thin film acting as bonding material between two crack faces. The neat sample had shiny, smooth crack surface which was expected as there is no material in between the crack faces.

Finite element analysis using ANSYS® showed good agreement with experimental results. For E_2 = 1 and 0.1 GPa (E_1 = 3.5 GPa, ν_1 = 0.2 and ν_2 = 0.3), 0 % healed sample showed variation in the stiffness values according to the crack length. Due to healed crack the stiffness values for 100 % healed samples with different crack lengths are almost same. For the value of E_2 = 0.01 GPa, 100 % healed samples showed almost same stiffness value as that of 0 % healed samples. This shows that healing of crack depends upon healed material properties.

Chapter 8

8.1 Conclusion

1. A new monomer (5E2N) with a suitable liquid temperature range was selected to replace DCPD monomer. Its ROMP behavior was investigated. The new monomer was successfully encapsulated in poly UF microcapsules.

2. Self-healing was achieved with the new monomer 5E2N without any external assistance for wide temperature range from -20 to 60 °C and vacuum test at 23 °C.

3. Preliminary thermal shock test results and vacuum test results showed that the 5E2N monomer can be a potential candidate for space application and can be selected for future work.

4. New approach using stiffness to determine healing performance is a good choice to compare healing efficiency among different types of samples.

5. This ANSYS® model is very flexible for analysis and can be used to determine healing performance for different material properties and crack lengths. The ANSYS® model can be useful to predict material property requirement of the healing material.

8.2 Contributions

The main aim of this thesis was to develop the self-healing material for the space applications. In the fulfillment of that following contributions were made in this thesis work.

- Finding a new monomer for use as healing agent for space applications
- Modify microencapsulation process to get good quality microcapsules
- Set manufacturing process to get good quality test samples
- Mechanical testing was carried out for different test conditions
- New approach (stiffness) was used to determine healing efficiency
- Experimental results were verified with analysis model using ANSYS®10.0
- Patent application is under progress for the outcome of this project work [40]
- Participated in the poster presentation at Canadian Space Agency [41]
- A paper was submitted for presentation of 1st International Conference on Self Healing Materials [42]

8.3 Recommendation for future work

Conclusion mentioned in section 8.1 was obtained for samples without fibers. Healing phenomenon can be studied using the samples containing fibers. Also healing performance can be tested in UV radiation and in atomic oxygen environment.

An alternative catalyst to replace Grubbs' catalyst can be investigated.

References

1. http://www.carbonfiber.gr.jp/english/tanso/images/plane01_b.jpg
2. http://mediaarchive.ksc.nasa.gov/search.cfm?cat=23
3. http://www.eads.com/xml/content/OF00000000400004/2/15/41328152.jpg
4. http://www.ceenet.org/workshops/lectures2002/Krzysztof_Muchorovski/Ceenet'02/satellite_ACTS.gif
5. http://launchspace.santasoft.com/1030.htm.
6. Issert C., Hoa S.V., Sedaghati R., "Self-healing materials and its potential applications" Project report. Concordia University, 2003.
7. Mehrholz D., Leushacke L. , Flury W., Jehn R., Klinkrad H., Landgraf M., "Detecting, Tracking and Imaging Space Debris", European Space Agency bulletin 109 , February 2002, pp.128-134.
8. Schonberg W. P., "Protecting Spacecraft Against Meteoroid/Orbital Debris Impact Damage: An Overview", Space Debris, Volume 1, Number 3, 1999, pp.195-210.
9. Trask R.S., Bond I.P., Semprimoschnig C., "Self-Healing Of Composite Structures In A Space Environment", *ICCM15 - 15th International Conference on Composite Materials*, Durban, South Africa. 27 June - 1 July 2005.
10. http://www.rand.org/pubs/monograph_reports/MR864/MR864.apB.pdf#search=%22cause%20of%20failure%20%2B%20spacecraft%22.
11. http://www.colorado.edu/ASEN/asen4012/MaterialsPapers/Selfhealing%20composites.pdf pp.44.

12. Kessler M.R., White S.R., "Self activated healing of delamination damage in woven composites", Composite part-A: Applied Science and Manufacturing 32:5, 2001, pp.683-699.
13. Kessler M.R., Sottos N.R. and White S.R. "Self-healing structural composite material". *Composites Part A:* Applied Science and Manufacturing. 2003, 34:8, pp.743-753.
14. White S.R., Sottos N.R., Geubelle P.H., Moore J.S., Kessler M.R., Sriram S.R., Brown E.N., Viswanathan S.: "Autonomic healing of polymer composites", Nature. 2001, 409, pp. 794-797.
15. Brown E. N., Sottos N. R., White S.R., "Fracture Testing of a Self-Healing Polymer Composite", Experimental Mechanics, vol.42, N.4, 2002, pp. 372-379.
16. Rule J.D., Sottos N.R., White S.R. and Moore J.S. "The Chemistry of Self-Healing Polymers", Education in Chemistry., 2005: 42:5, pp.130-132.
17. Bleay S.M., Loader C.B., Hawyes V.J., Humberstone L., Curtis P.T., "A smart repair system for polymer matrix composites" Composites - Part A - Applied Science and Manufacturing, 2001,v.32, n.12, pp.1767-1776.
18. Pang J.W.C., Bond I.P., " Bleeding Composites-damage detection and self repair using a biomimetic approach, Comporsites:Part A , 36 (2005), pp.183-188.
19. Zako M., Takano N., "Intelligent material systems using epoxy particles to repair microcracks and delamination damage in GFRP", Journal of Intelligent Material Systems and Structures. 1999 , v. 10 , n. 10 , pp. 836-841.

20. Chen X., Dam M.A., Ono K., Mal A., Shen H., Nutt S.R., Sheran K., Wudl F. "A Thermally Re-mendable Cross-Linked Polymeric Material", Science 2002, 295, pp.1698-1702.

21. http://www.chem.ucla.edu/dept/Organic/wudl.html.

22. Thomas A.P., Alireza V.A., Diego A., Syrus C., Nemat-Nasser, Sia Nemat-Nasser, " Self Healing Structural Composites with Electromagnetic functionality", SPIE 2003.

23. Therriault D., Scott R.W., Jennifer A.L. "Chaotic mixing in three-dimensional microvascular networks fabricated by direct-write assembly". Published online: 23 March 2003, doi:10.1038/nmat863, pp. 265-266.

24. Issue of a leading UK newspaper, the Guardian, May 13, 2004 (http://www.guardian.co.uk/life/feature/story/0,13026,1215056,00.html).

25. Brown E.N., Kessler M.R., Sottos N. R. and White S. R. "In situ poly (urea-formaldehyde) microencapsulation of dicyclopentadiene", Journal of Microencapsulation, 2003; 20:6, pp. 719-730.

26. Kessler M. R. and White S.R.: "Cure kinetics of the ring-opening metathesis polymerization of dicyclopentadiene", *Journal of Polymer Science Part A-Polymer Chemistry*. 2002; 40:14, 2373-2383.

27. Guntzburger Y., " Multifunctional System enabling Self-Healing of Spacecraft Structures for the Mitigation of Damage", Investigation Report, Concordia University, June 24, 2006, pp.1-26.

28. http://www.swri.edu/3pubs/ttoday/summer95/microeng.htm.

29. http://www.csl.gov.uk/prodserv/rds/pesticide/micro.cfm.

30. Brown E.N., White S. R. and Sottos N. R. "Microcapsule induced toughening in a self-healing polymer composite", Journal of Materials Science, 2004; 39, pp.1703-1710.

31. Beres W, Koul A. K., Thamburaj R., " A tapered Double-Cantilever-Beam Specimen Designed for Constant-K Testing at Elevated Temperatures", Journal of Testing and evaluation, JTEVA, Vol. 25, No. 6, November 1997, pp. 536-542.

32. Mostovoy S., Crosley P.B., Ripling E.J., " Use of Crack Line-Loaded Specimens for Measuring Plane-Strain Fracture Toughness", Journal of Materials, v. 2, n.3, September 1967, pp. 661-681.

33. Owen M.J., Rose R.G., "The Fracture Toughness and Crack Propagation Properties of Polyester Resin casts and laminates", Journal of Physics D and Applied Physics, v.6, 1973, pp. 42-53.

34. Freed C.N., Kraft J.M., "Effect of Side Grooving on Measurements of Plain strain fracture Toughness". Journal of Materials, V1, 1966, pp. 770-790.

35. http://science.ksc.nasa.gov/pao/faq/faqanswers.htm (NASA, FAQ).

36. Guntzburger Y., "Multifunctional system enabling self-healing of spacecraft structures for the mitigation of damage: Improvement of self healing system", Internship report, Concordia University, November 2005, pp. 1-13.

37. ANSYS®10.0, Inc. Canonsburg, USA.

38. http://www.oulu.fi/atkk/tkpalv/unix/ansys-6.1/content/Hlp_E_SOLID92.html.

39. http://www.oulu.fi/atkk/tkpalv/unix/ansys-6.1/content/Hlp_E_SOLID186.html.

40. Thatte G., Hoa S. V., Philippe G. M., Guntzburger Y., Haddad E., " Self Healing Composite Material", Patent Application No. 60/829,689, October 2006.

41. Thatte G., Hoa S. V., Philippe G. M., Haddad E., " Development and Characterization of Self-Healing Epoxy Systems for Space Applications", Presented at Canadian Space Agency (CSA), October 2006.

42. Thatte G., Hoa S. V., Philippe G. M., Haddad E., " Self Healing Composite Materials for Space Applications : 1st International Conference on Self Healing Materials, Noordwijk, The Netherlands, April 2007.